



This is a repository copy of *All-acrylic film-forming colloidal polymer/silica nanocomposite particles prepared by aqueous emulsion polymerization*.

White Rose Research Online URL for this paper:  
<http://eprints.whiterose.ac.uk/79025/>

---

**Article:**

Fielding, L.A., Tonnar, J. and Armes, S.P. (2011) All-acrylic film-forming colloidal polymer/silica nanocomposite particles prepared by aqueous emulsion polymerization. *Langmuir*, 27 (17). 11129 - 11144. ISSN 0743-7463

<https://doi.org/10.1021/la202066n>

---

**Reuse**

Unless indicated otherwise, fulltext items are protected by copyright with all rights reserved. The copyright exception in section 29 of the Copyright, Designs and Patents Act 1988 allows the making of a single copy solely for the purpose of non-commercial research or private study within the limits of fair dealing. The publisher or other rights-holder may allow further reproduction and re-use of this version - refer to the White Rose Research Online record for this item. Where records identify the publisher as the copyright holder, users can verify any specific terms of use on the publisher's website.

**Takedown**

If you consider content in White Rose Research Online to be in breach of UK law, please notify us by emailing [eprints@whiterose.ac.uk](mailto:eprints@whiterose.ac.uk) including the URL of the record and the reason for the withdrawal request.



[eprints@whiterose.ac.uk](mailto:eprints@whiterose.ac.uk)  
<https://eprints.whiterose.ac.uk/>

# All-acrylic film-forming colloidal polymer/silica nanocomposite particles prepared by aqueous emulsion polymerization

Lee A. Fielding, Jeff Tonnar and Steven P. Armes\*

Dainton Building, Department of Chemistry, The University of Sheffield, Brook Hill, Sheffield, S3 7HF, UK.

**Abstract.** The efficient synthesis of all-acrylic, film-forming, core-shell colloidal nanocomposite particles via in situ aqueous emulsion copolymerization of methyl methacrylate with n-butyl methacrylate in the presence of a glycerol-functionalized ultrafine silica sol using a cationic azo initiator at 60 °C is reported. It is shown that relatively monodisperse nanocomposite particles can be produced with typical mean weight-average diameters of 140 - 330 nm and silica contents of up to 39 wt. %. The importance of surface functionalization of the silica sol is highlighted and it is demonstrated that systematic variation of parameters such as the initial silica sol concentration and initiator concentration affect both the mean particle diameter and the silica aggregation efficiency. The nanocomposite morphology comprises a copolymer core and a particulate silica shell, as determined by aqueous electrophoresis, x-ray photoelectron spectroscopy and electron microscopy. Moreover, it is shown that films cast from n-butyl acrylate-rich copolymer/silica nanocomposite dispersions are significantly more transparent than those prepared from the poly(styrene-co-n-butyl acrylate)/silica nanocomposite particles reported previously. In the case of the aqueous emulsion homopolymerization of methyl methacrylate in the presence of ultrafine silica, a particle formation mechanism is proposed to account for the various experimental observations made when periodically sampling such nanocomposite syntheses at intermediate comonomer conversions.

\* Author to whom correspondence should be addressed (s.p.arnes@sheffield.ac.uk)

## Introduction

Organic-inorganic nanocomposite particles, in particular systems comprising of polymer chains and silica, are of considerable academic and industrial interest. For example, film-forming copolymer/silica nanocomposite particles are currently manufactured as additives for exterior façade coatings.<sup>1</sup> Such façade coatings exhibit superior dirt-shedding properties, better uv resistance and enhanced blocking resistance.<sup>2</sup> Several review articles on the academic advances in this sub-field have recently been published.<sup>3-6</sup>

In principle, colloidal nanocomposite particles can be prepared simply by heteroflocculation between a pre-formed latex and a silica sol.<sup>7-9</sup> However, particles prepared by such systems have been demonstrated to show reversible silica adhesion<sup>8,9</sup> and low transparency when cast as a film.<sup>10</sup> It has been widely reported that in situ (co)polymerization of various vinyl monomers in the presence of ultrafine silica sols either in aqueous solution,<sup>10-31</sup> in alcohol/water mixtures<sup>32-36</sup> or in purely alcoholic media<sup>37-40</sup> can result in the formation of vinyl polymer/silica nanocomposite particles. For example, Barthelet et al.<sup>15</sup> described the free radical (co)polymerization of 4-vinylpyridine (4VP) using ammonium persulfate in the presence of an ultrafine silica sol. The resulting colloidal nanocomposite particles had mean diameters of 150 to 170 nm and silica contents as high as 37 % by mass. Subsequent solid-state NMR studies suggest that an acid-base interaction between the pendent pyridine rings on the polymer chains and the surface silanol groups on the silica nanoparticles most likely promotes nanocomposite formation.<sup>22</sup> Percy et al. demonstrated that the particle size and silica content of these P4VP/silica nanocomposite particles were surprisingly insensitive to the reaction conditions.<sup>16</sup> The combination of transmission electron microscopy (TEM), x-ray photoelectron spectroscopy (XPS) and electron spectroscopy imaging provided compelling evidence for a ‘currant-bun’ morphology.<sup>17,21</sup> Statistical copolymerization of 4VP with either styrene, methyl methacrylate (MMA) or n-butyl acrylate (BuA) also produced colloidal nanocomposite particles.<sup>16,17</sup> In the latter case, the resulting copolymer/silica nanocomposite particles could be cast into transparent films with silica contents of up to 56 wt. %.

In 2004 Chen et al. described the synthesis of PMMA/Silica nanocomposite particles containing at least 10 mol. % 1-vinylimidazole.<sup>11</sup> These particles had ‘raspberry’ morphologies with mean diameters ranging from 120 to 350 nm and silica contents of 5 to 47 % by mass. This work was subsequently extended when similar nanocomposite particles were also obtained using cationic 2-(methacryloyl)ethyltrimethyl ammonium chloride as a

comonomer instead of 1-vinylimidazole.<sup>27</sup> Nanocomposite particles comprising silica cores and polymeric shells were reported by Cheng et al.<sup>41</sup> Again, an acid-base interaction between the 4VP (co)monomer and the silica component was utilized to aid particle formation. However, auxiliary (co)monomers such as 4VP are undesirable for industrial applications of nanocomposite particles due to their additional cost and malodorous nature.

Qi et al. reported the synthesis of a series of ‘raspberry-like’ poly(methyl methacrylate-co-n-butyl acrylate)/silica nanocomposite particles by in situ emulsion copolymerization.<sup>42</sup> Silica contents could be varied but this formulation required the use of additional surfactants such as nonylphenol poly(oxyethylene) or sodium dodecyl sulfate to ensure nanocomposite formation. Solvent extraction studies suggested that around 15 % of the 15 nm silica particles became grafted to the copolymer chains during nanocomposite formation. Unfortunately, the addition of surfactants can often compromise film integrity and optical clarity, since these species can migrate through the film on drying, leading to undesirable segregation.<sup>43</sup>

Colver et. al.<sup>31</sup> reported the so-called ‘Pickering emulsion polymerization’ of MMA in the presence of a 25 nm silica sol to form colloiddally stable nanocomposite particles. In this formulation, precise control over the solution pH was essential; optimal results were obtained at pH 5.5, whereas attempted syntheses at pH 10 led to coagulation of bare latex particles while broad particle size distributions were obtained at pH 3. Although not mentioned by Colver et al., ultrafine silica sols often exhibit a minimum in colloidal stability at around pH 5.5,<sup>44</sup> which may well explain their observations. We have successfully repeated this synthesis protocol in our laboratory. However, a major drawback of this formulation (at least in our hands) is its relatively low silica aggregation efficiency, i.e. not all of the silica sol in the reaction medium is incorporated into the final nanocomposite particles leaving significant excess silica in solution; this is likely to be detrimental for most, if not all, potential applications. It is also debatable whether the term ‘Pickering emulsion polymerization’ is really an appropriate description for such syntheses, since there is no correspondence between the initial micrometer-sized silica-stabilized monomer droplets and the final submicrometer-sized PMMA/silica nanocomposite particles.

A significant problem often associated with the in situ polymerization route to polymer/silica nanoparticles is the relatively low silica aggregation efficiency achieved during nanocomposite formation. The excess silica sol remains in solution and generally has to be

removed by time-consuming centrifugation-redispersion cycles, which is simply impracticable on an industrial scale. Moreover, the presence of excess silica sol compromises the performance of certain nanocomposite particles when used as pH-responsive Pickering emulsifiers,<sup>45</sup> as well as causing reduced transparency and embrittlement in solvent-cast nanocomposite films.<sup>10</sup> However, nanocomposite syntheses that achieve high silica aggregation efficiencies have been recently reported. For example, Dupin et al.<sup>30</sup> described the surfactant-free preparation of poly(2-vinylpyridine)/silica colloidal nanocomposite particles via aqueous emulsion (co)polymerization using a commercial 20 nm aqueous silica sol as the sole stabilizing agent and a cationic azo initiator. The resulting particles had a well-defined core-shell morphology (polymer core, silica shell), with mean particle diameters ranging between 180 and 220 nm, and silica aggregation efficiencies of up to 88 – 99 %. More recently, Schmid et. al.<sup>29,46</sup> reported a highly efficient surfactant-free formulation for the preparation of colloidal polystyrene/silica nanocomposite particles with well-defined core-shell particle morphologies and up to 95 % silica aggregation efficiency. These nanocomposite particles had mean diameters ranging from 200 to 400 nm and contained 22 to 28 % silica by mass. In this formulation, the key to success is the use of a commercially available glycerol-functionalized aqueous silica sol (Bindzil CC40) in combination with a cationic azo initiator.

Most film-forming nanocomposite syntheses to date have either involved the use of miniemulsion polymerization,<sup>47-49</sup> undesirable auxiliary (co)monomers,<sup>17</sup> alcoholic silica sols<sup>33,40</sup> or in situ functionalization of the silica sol.<sup>48,49</sup> Schmid et al. extended their glycerol-functionalized silica sol formulation to include film-forming poly(styrene-co-n-butyl acrylate)/silica colloidal nanocomposite particles.<sup>10</sup> This route offered a potentially useful advance over earlier syntheses since it does not involve expensive auxiliary comonomers, added surfactants or volatile organic compounds. The nanocomposite particles comprised up to 38 % silica by mass, with silica aggregation efficiencies exceeding 95 %. Upon drying the nanocomposite dispersions, highly transparent free-standing films were obtained. Moreover, control experiments confirmed that the in situ copolymerization route is far superior to simple ad-mixtures of film-forming latex and the glycerol-functionalized silica sol, since the latter approach only produces relatively opaque films.

Herein the synthesis of an all-acrylic colloidal nanocomposite formulation is reported. Thus a series of poly(methyl methacrylate-co-n-butyl acrylate)/silica particles were synthesized by in

situ aqueous emulsion copolymerization of varying proportions MMA and BuA in the presence of an aqueous glycerol-functionalized ultrafine silica sol using a cationic azo initiator at 60 °C. These nanocomposite particles were then characterized in terms of their particle size, silica content, surface composition and film formation behavior and the data compared to previous nanocomposite formulations.

## **Experimental Section**

### **Materials**

MMA and BuA were purchased from Aldrich, passed in turn through a basic alumina column to remove inhibitor and stored at -20 °C prior to use. 2,2'-Azobis(isobutyramidine) dihydrochloride (AIBA) was used as received from Aldrich. Glycerol-functionalized silica sol (Bindzil CC40; 37 wt. % aqueous dispersion; 12 nm nominal diameter) was supplied by Eka Chemicals (Bohus, Sweden), which is a division of AkzoNobel (Netherlands). BET measurements indicated that the silica particles have a specific surface area of 158 m<sup>2</sup> g<sup>-1</sup>. Given a silica sol density of 2.16 g cm<sup>-3</sup> (as determined by helium pycnometry), this suggests a mean diameter of 18 nm, which is consistent with TEM studies. Deionized water obtained from an Elgastat Option 3A water purifier was used in all experiments.

### **Nanocomposite Synthesis**

The following copolymerization is a representative example of particle synthesis. Aqueous Bindzil CC40 silica sol (7.5 g) was diluted with water (33.5 g) in a round-bottomed flask, MMA and BuA (5.00 g total monomer mass in varying ratios) was added and the solution was degassed with bubbling N<sub>2</sub>. This was heated to 60 °C followed by the addition of 150 mg AIBA initiator dissolved in 4.0 g water to give a total mass of water of 45 g at pH 8. Each polymerization was allowed to proceed for 24 h under a positive nitrogen atmosphere. The resulting colloidal dispersions were purified by repeated centrifugation-redispersion cycles, with each successive supernatant being decanted and replaced with water. Initial silica and initiator concentrations were varied systematically to investigate their effects particle synthesis and comonomer ratios ranging from 100:0 to 30:70 MMA to BuA were studied. Control experiments were carried out by conducting reactions either with no silica sol, non-functionalized silica sols or cationic initiator. In order to investigate the mechanism of particle formation, scaled-up syntheses were conducted on a 500 g scale whereby aliquots of the reaction mixture were withdrawn and exposed to air before analysis.

## **Characterization of Nanocomposite Particles and Films**

Dynamic light scattering (DLS) studies were conducted at 25 °C using a Malvern Zetasizer Nano ZS instrument equipped with a 4 mW He-Ne solid-state laser operating at 633 nm. Back-scattered light was detected at 173° and the mean particle diameter was calculated over thirty runs of ten seconds duration from the quadratic fitting of the correlation function using the Stokes-Einstein equation. All measurements were performed in triplicate on highly dilute aqueous dispersions. Disk centrifuge photosedimentometry (DCP) was used to determine weight-average particle size distributions. The disk centrifuge (CPS Instruments DC24000 instrument) was operated between 16,000 and 24,000 rpm and the spin fluid comprised a density gradient built from 8.0 to 24.0 wt. % aqueous sucrose solutions; a small volume of n-dodecane (0.5 mL) was used in order to extend the gradient lifetime. The disk centrifuge was calibrated with a poly(vinyl chloride) latex with a weight-average particle diameter of 263 nm. Solid-state nanocomposite densities were determined by helium pycnometry (Micromeritics AccuPyc 1330 instrument). Solids contents were determined gravimetrically (Ohaus M45 moisture analyzer) at a drying temperature of 150 °C. Thermogravimetric analysis (TGA; TA Instruments Q500) was conducted on freeze-dried particles which were heated in air up to 800 °C at a heating rate of 20 °C min<sup>-1</sup>. The observed mass loss was attributed to complete pyrolysis of the copolymer component, with the remaining incombustible residues being attributed to pure silica. TEM (Phillips CM100 instrument operating at 100 kV) studies were conducted on samples prepared by drying a drop of dilute aqueous dispersion on a carbon-coated copper grid. Field emission scanning electron microscopy images (FE-SEM, FEI Inspect instrument operating at 20 to 30 kV) were obtained from samples dried onto carbon disks and sputter-coated with gold. Aqueous electrophoresis measurements (Malvern Zetasizer NanoZS instrument) were conducted in the presence of 1.0 mM KCl as a background salt. The solution pH was initially adjusted to pH 11 by the addition of KOH and subsequently titrated to pH 1.5 using HCl. Nanocomposite film transparencies were assessed by visible absorption spectrophotometry (Perkin-Elmer Lambda 25 spectrometer) between 190 to 1100 nm using a scan speed of 960 nm min<sup>-1</sup>. Fourier transform infra-red spectra (FT-IR, Thermo Nicolet iS10) were recorded for freeze-dried nanocomposite particles using a diamond ATR sampling accessory. <sup>1</sup>H NMR spectra were recorded for freeze-dried nanocomposite samples dissolved in CDCl<sub>3</sub> using a 400 MHz Bruker Avance-400 spectrometer. XPS studies were conducted on freeze-dried nanocomposite particles pressed onto indium foil using a Kratos Axis Ultra 'DLD'

instrument equipped with a monochromatic Al K $\alpha$  X-ray source ( $h\nu = 1486.6$  eV) operating at a base pressure in the range of  $10^{-8}$  to  $10^{-10}$  mbar.

## Results and Discussion

The combination of a glycerol-functionalized silica sol and a cationic azo initiator has already been reported to produce poly(styrene-co-n-butyl acrylate)/silica particles in aqueous media.<sup>10,29</sup> Such nanocomposite particles possess a well-defined core-shell morphology and have relatively narrow particle size distributions. Furthermore, this robust formulation leads to very high silica aggregation efficiencies without requiring either auxiliary (co)monomers, surfactants or non-aqueous (co)solvents.

The glycerol-functionalized silica sol (Bindzil CC40) is manufactured by reacting the surface silanol groups of a conventional silica sol with 3-glycidoxypropyl trimethoxysilane.<sup>50</sup> Ring-opening of the glycidyl group occurs simultaneously with hydrolysis of the siloxane groups to produce a highly hydrophilic glycerol group. According to the manufacturer, the surface coverage of the silica particles is one to two silane molecules per nm<sup>2</sup> surface area. Such glycerol-decorated silica sols are claimed<sup>50</sup> to have higher colloidal stability under certain conditions, e.g. in the presence of excess surfactant, added salt etc. In our experience, the surface glycerol groups are essential for efficient nanocomposite syntheses, since control experiments utilizing non-functionalized silica sols of similar size merely contain mainly latex particles with substantial quantities of excess silica sol, as judged by TEM studies.<sup>29</sup> Solid-state NMR studies have previously been used to characterize the interface between the organic and inorganic components of poly(styrene-co-n-butyl acrylate)/silica particles prepared with glycerol-functionalized silica sol.<sup>51</sup> It was shown that the aliphatic acrylate protons are preferentially located at the surface of the silica particles, suggesting that there is a specific interaction between these residues and the glycerol-functionalized silica surface. Hydrogen bonding between the glycerol hydroxyl groups and the acrylate ester carbonyls appears to be the most likely explanation for this observation.<sup>51</sup>

As an extension of this earlier work, an all-acrylic colloidal nanocomposite formulation has been developed based on the aqueous emulsion copolymerization of MMA and BuA using the same cationic azo initiator and glycerol-functionalized silica sol as described previously. A schematic representation of this route is shown in Figure 1 and summaries of the various nanocomposite formulations are detailed in Tables 1 and 2. One motivation for the present

study was to extend this formulation to all-acrylic comonomers since this was expected to improve nanocomposite film transparency.

### **Synthesis of PMMA/silica particles**

Initially, PMMA/silica nanocomposite particles were synthesized according to the previously reported protocol<sup>29</sup> with styrene monomer being replaced by MMA. Although of no obvious commercial utility, this homopolymer/silica nanocomposite formulation was expected to be more amenable to characterization by electron microscopy due to the relatively high glass transition temperature of the PMMA chains.

The silica sol concentration was systematically varied in the nanocomposite formulation in order to optimize the silica aggregation efficiency. More specifically, a series of PMMA/silica nanocomposite particles were prepared using between 0.5 and 4.0 g dry weight of 18 nm glycerol-functionalized silica sol with fixed amounts of MMA monomer (5.00 g) and AIBA initiator (50.0 mg) in a constant reaction mass of 50 g at 60 °C (Table 1, entries 2-9). High monomer conversions were obtained in all cases (as judged by gravimetry) and the colloidal stability and polydispersity of the resulting nanocomposite particles were assessed by DLS and DCP.

Stable nanocomposite dispersions were obtained in all cases above a certain critical silica sol concentration, below which flocculation occurs (see entries 2 and 3). Entry 4 demonstrates that optimization of the silica sol concentration can lead to highly efficient silica aggregation, with very little excess silica sol being present in the reaction solution as judged by TEM. As the silica sol concentration is increased (entries 4 – 9) the mean silica content of the nanocomposite particles remains relatively consistent at around 25 to 30 % by mass. This inevitably leads to lower silica aggregation efficiencies, meaning that increasing amounts of excess silica sol are present in the final nanocomposite dispersions. This excess silica can be removed by repeated centrifugation-redispersion cycles but this is both time-consuming and inefficient. Particle densities determined by helium pycnometry range from 1.36 to 1.44 g cm<sup>-3</sup>; these values correlate well with densities estimated from the silica contents measured by TGA.

Intensity-average and weight-average diameters of PMMA/silica nanocomposite dispersions were determined by DLS and DCP, respectively (see Table 1). As expected, the weight-

average particle diameters determined by DCP are smaller than the intensity-average diameters determined by DLS. The former diameters ranged between 242 and 271 nm whilst the latter were typically of the order of 200 nm. Neither technique provides much evidence for flocculation, suggesting that reasonably good colloidal stabilities are achieved. Earlier work by Schmid et al.<sup>29</sup> on the analogous polystyrene/silica nanocomposite particles prepared via this route indicated that somewhat smaller nanocomposite particles were obtained at higher silica concentrations; this trend was not discernible in the present study.

The mean particle diameters obtained in the present work are significantly lower than those reported for polystyrene/silica particles, which typically had weight-average diameters of approximately 300 nm. At first glance, this difference could be simply attributed to replacing styrene with MMA. However, a key difference between the two experimental protocols is that overhead stirring was implemented in the current work, whereas magnetic stirring was used in the previous work. Thus the more efficient agitation achieved with overhead stirring might well account for the observed variation in particle size. To test this hypothesis, a series of PMMA/silica particles were synthesized using magnetic stirring (see Table 1, entries 10 - 16). These experiments demonstrate that, as the silica sol concentration is increased, the silica aggregation efficiency is reduced. However, the weight-average particle diameters are now 274-329 nm, which is comparable to that observed for the polystyrene/silica formulation by Schmid et al.<sup>29</sup> Moreover, there is a modest reduction in particle diameter at higher silica sol concentrations. This suggests that both the stirring efficiency and the initial silica concentration can be utilized to target the desired nanocomposite particle diameter.

To investigate the effect of initiator concentration on particle formation, a series of PMMA/silica nanocomposite particles were prepared using 25 – 150 mg AIBA initiator at a fixed silica sol concentration (see entries 6 and 17 – 19 in Table 1). In each case, colloidally stable nanocomposite particles were formed with weight-average particle diameters consistently around 200 nm with fairly narrow particle size distributions. The particle size appears to be relatively insensitive to the initiator concentration, but silica aggregation efficiencies increased from 61 % with 25 mg AIBA to 93 % when using 150 mg AIBA. Schmid et al.<sup>29</sup> confirmed that the AIBA initiator is electrostatically adsorbed onto the glycerol-functionalized silica sol, with an adsorbed amount of 0.045 mg m<sup>-2</sup> being observed at 20 °C in the absence of any monomer. For the formulations presented in this work (for which 2.5 g silica is used), this adsorbed amount corresponds to an initiator mass of only 20

mg AIBA. Assuming that the initiator adsorption has negligible temperature dependence, this means that  $\sim 130$  mg of soluble (i.e. non-adsorbed) initiator is present in all nanocomposite particle synthesis. Indeed, in the previous polystyrene/silica nanocomposite study<sup>29</sup> it was found that, when less than  $0.045 \text{ mg m}^{-2}$  of initiator was used, ‘patchy’ nanocomposite particle surfaces were observed (along with low silica aggregation efficiencies). It was also suggested that surface polymerization might play an important role in nanocomposite formation. In the present study, all nanocomposite syntheses have been conducted under conditions which involve a significant excess of soluble AIBA initiator, since this seems to favor the highest silica aggregation efficiencies.

Representative TEM images of PMMA/silica nanocomposite particles prepared by aqueous emulsion polymerization are shown in Figure 2. Images A and B show particles after excess non-adsorbed silica sol has been carefully removed by repeated centrifugation, whereas images C and D were recorded by simply diluting the reaction solution. Image C shows the diluted reaction solution of a formulation with relatively high silica aggregation efficiency (see entry 5 in Table 1). In contrast, image D confirms the presence of a significant amount of excess silica sol for a formulation with a relatively low silica aggregation efficiency (see entry 6 in Table 1). Thus TEM is very useful for qualitatively judging the extent of contamination of the nanocomposite particles by excess, non-adsorbed silica sol. It is emphasized that this excess silica must be carefully removed before any meaningful characterization of the nanocomposite particles can be undertaken.

In all cases, close inspection of these TEM images confirm the presence of the 18 nm silica particles located at the surface of the PMMA/silica nanocomposite particles. The surface coverage appears to be relatively high, with little or no sign of any bare patches of underlying latex. The colloidal stability of these nanocomposite dispersions derives from the charge stabilization conferred by the anionic adsorbed silica particles. The nanocomposite surface is consistent with either a ‘core-shell’ or ‘raspberry’ particle morphology but unfortunately conventional TEM studies cannot easily differentiate between these two possibilities.

Control experiments were conducted in which either no silica sol, non-functionalized silica sols or an anionic initiator were utilized, while fixing all other parameters (see entries 1 and 20 - 22 in Table 1). When no silica sol is used, only rather polydisperse charge-stabilized PMMA latexes are obtained (Figure 3A). In this case, the cationic surface charge is conferred

by the AIBA initiator fragments. When non-functionalized silica sols (e.g. either Ludox TM-40 or Bindzil 2040; see Figures 3B and C respectively) are used, there is little or no interaction between the organic and inorganic components and hence no compelling evidence for successful nanocomposite particle formation. Using anionic persulfate initiator instead of AIBA produced only coagulated particles, rather than a stable colloidal dispersion (see Figure 3D). Thus these control experiments demonstrate that the combination of glycerol-functionalized silica sol with the cationic AIBA initiator is essential to produce well-defined nanocomposite particles with high silica aggregation efficiencies.

### **Synthesis of film-forming P(MMA-BuA)/silica particles**

Film-forming nanocomposite particles were prepared by copolymerizing increasing amounts of BuA with MMA in order to lower the  $T_g$  of the copolymer chains. The effect of varying the (co)monomer feed ratio is summarized in Table 2 (see entries 1 - 7). For each formulation, the particles were synthesized using 2.80 g of glycerol-functionalized silica sol in a fixed reaction mass of 50 g at 60 °C; total (co)monomer was fixed at 5.00 g while the MMA:BuA comonomer ratio was varied from 90:10 to 30:70 by mass. Stable nanocomposite dispersions were obtained in all cases, except for the highest proportion of BuA, where flocculation was observed. The average silica content of the nanocomposite particles varied between 21 and 33 wt. % with silica aggregation efficiencies ranging from 50 to 90 %. Particle densities were somewhat lower than those of the PMMA/silica nanocomposite particles; this is due to the lower silica contents of these particles. The increasing BuA content of these copolymer/silica nanocomposites was confirmed by FT-IR studies on freeze-dried samples (Figure S1, Supporting Information): the C-H bands at 2995 and 2841  $\text{cm}^{-1}$  due to MMA residues become less prominent, while the band at 2874  $\text{cm}^{-1}$  attributed to the C-H stretch of the BuA residues gradually becomes more intense. Furthermore, the composition of the copolymer chains within the nanocomposite particles was readily calculated using  $^1\text{H}$  NMR spectroscopy (Figure S2 and Table S1, Supporting Information). For higher levels of BuA in the comonomer feed, the  $\text{OCH}_2$  signal at 3.80 - 4.20 ppm increases whereas the  $\text{OCH}_3$  signal due to the MMA residues at 3.50 - 3.75 ppm is reduced. Assuming the copolymer is fully dissolved in the solvent and no polymer chains remain bound to the surface of the silica particles, integration of these two signals provides the molar (and hence weight) ratios of the individual comonomers within the copolymer chains. These values are generally in good agreement with the feed ratios.

Figure 4 shows the particle size distributions of selected copolymer/silica nanocomposite particles obtained by DCP. In each case the particle size distribution is narrow and there is little or no sign of particle flocculation (the weak shoulders observed at larger diameters merely correspond to doublets). Similarly, DLS studies indicate mean nanocomposite particle diameters of between 240 and 280 nm with relatively low polydispersities (see Table 2, entries 1 – 6). This latter technique reports an intensity-average diameter, which is necessarily always larger than the weight-average diameter reported by DCP for particles of finite polydispersity.

Representative TEM images are shown in Figure 5 for MMA-rich nanocomposite particles, which remain well-defined after drying dilute aqueous dispersions at ambient temperature. Moreover, the particle surface is clearly coated with silica. As more BuA (co)monomer is introduced, the nanocomposite particles begin to coalesce on the TEM grid. This is expected, as the lower copolymer  $T_g$  promotes film formation during drying. In previous work<sup>10</sup> it was demonstrated that, as BuA comonomer is progressively incorporated into a styrene-based nanocomposite formulation, the mean silica content rose from 27 to 39 wt.%. This higher silica content correlated with the smaller nanocomposite particles produced when using higher proportions of BuA comonomer, which is consistent with the observed core-shell particle morphology.<sup>10</sup> However, the all-acrylic film-forming copolymer formulation employed in the present study produced somewhat lower silica contents of around 20 wt. % (see entries 11 and 12 in Table 2).

For an initial silica sol mass of 2.8 g, the silica aggregation efficiency was relatively low (see Table 2, entries 1 – 6). To investigate whether a higher silica aggregation efficiency could be achieved for the copolymer/silica nanocomposite particles prepared using a 50:50 comonomer feed ratio, the initial silica concentration was systematically reduced from 2.8 g to 0.90 g (Table 2, entries 5, 9 – 12). As expected,<sup>10</sup> substantial flocculation occurs below a certain critical silica sol concentration. When 1.90 g silica was utilized (see entry 11), stable particles are produced with a weight-average mean diameter of 205 nm but the silica aggregation efficiency is only 69 %. This suggests that excess silica is required for the successful synthesis of BuA-rich copolymer/silica nanocomposite particles. To examine whether a higher initial silica sol concentration enables the synthesis of nanocomposite particles with higher BuA content, the synthesis of copolymer/silica nanocomposite particles containing 70 % BuA by mass was attempted using 3.70 g silica (see entry 8 in Table 2).

Colloidally stable particles with an intensity-average diameter of 180 nm and a low polydispersity were obtained with this formulation. However, TEM studies of the unpurified reaction solution confirmed that excess silica is present. Such excess silica is expected to be detrimental to nanocomposite film properties if it is not removed prior to film formation, since it causes embrittlement and reduced transparency.<sup>10</sup>

### **Surface Characterization**

The surface compositions of selected nanocomposite particles were studied by both aqueous electrophoresis and x-ray photoelectron spectroscopy. Zeta potential versus pH curves are shown for both PMMA/silica and 50:50 P(MMA-BuA)/silica nanocomposite particles, along with the pristine glycerol-functionalized silica sol (see Figure 6). In all cases, negative zeta potentials were obtained throughout the pH range investigated. The rather similar electrophoretic behavior observed for the nanocomposite particles and the pristine silica sol suggests that the former particles have a silica-rich surface. This conclusion is in good agreement with the TEM images shown in Figures 2 and 5.

It might be expected that nanocomposite particles with a silica-rich surface should exhibit electrophoretic behavior comparable to that of the pristine sol. However, the copolymer/silica nanocomposite particles are actually more anionic than the pristine silica sol. This is not the first time such an observation has been reported; polystyrene/silica nanocomposite particles prepared by alcoholic dispersion polymerization<sup>40</sup> also exhibited more anionic character than the corresponding pristine sol and it remains unclear why this is the case. In view of the distinctive raspberry morphology exhibited by the nanocomposite particles, it is possible that surface roughness may play an important role but further work is required to clarify this issue.

XPS has a typical sampling depth of 2 to 10 nm.<sup>21,52</sup> This allows elemental surface compositions to be obtained for the near-surface of colloidal nanocomposite particles and films.<sup>21,29,52</sup> Figure 7 shows the XPS survey spectrum recorded for freeze-dried 50:50 P(MMA-BuA)/silica particles pressed onto indium foil. This spectrum has Si2p and Si2s signals at 104 and 155 eV respectively, which indicates the presence of silica at the surface of the nanocomposite particles. The silicon surface content is 11.3 atom %, which is significantly higher than the bulk silicon content of 3.2 atom % calculated from TGA data. This confirms that the nanocomposite particles have a silica-rich surface, which is consistent with the zeta potential data discussed above. Similar results were also reported by Schmid et

al.<sup>10</sup> for poly(styrene-co-n-butyl acrylate)/silica nanocomposite particles. The XPS survey spectrum of the 50:50 P(MMA-BuA)/silica particles shown in Figure 7 indicates a Si/C atomic ratio of 0.18, which is significantly higher than the bulk Si/C atomic ratio of 0.11 calculated from TGA. Again, this is consistent with a silica-rich surface composition. However, the former value is relatively low when compared to those obtained for freeze-dried MMA-rich nanocomposite samples (see Figure S3, Supporting Information). Thus the Si/C atomic ratio increases up to a maximum of 0.99 for a 90:10 P(MMA-BuA)/silica nanocomposite. This indicates that less copolymer is located at the surface of the higher  $T_g$  nanocomposite particles. This is consistent with reduced copolymer chain mobility, which inevitably leads to a higher proportion of the hydrophilic silica particles remaining at the surface.

On close inspection, the C1s signal shown in Figure 7 is significantly more intense than that recorded for the pristine glycerol-functionalized silica sol (61 at. % compared to 12 at. % for the silica sol). This suggests that the copolymer chains are also present at the nanocomposite film surface. Peak deconvolution of the C1s core-line spectra (see inset in Figure 7) reveals the presence of C-C, C-O and C=O species at the surface of the nanocomposite particles. The latter species is due to the ester carbonyls in the MMA and BuA comonomers, which confirms that the copolymer chains are located at the interface. However, further interpretation is difficult, because the surface glycerol groups on the silica particles also contribute to the C-C and C-O signals.

### **Selective Removal of Polymeric and Silica Components**

Since TEM, XPS and aqueous electrophoresis provide compelling evidence that the nanocomposite particles have a silica-rich surface, it is likely that they possess either a ‘core-shell’ or a ‘raspberry’ morphology.<sup>4</sup> To determine their actual morphology, either the copolymer or the silica components can be selectively removed. Removal of the copolymer simply involves calcination at 500 °C, since this pyrolyses the organic component but leaves the refractory silica intact. Figure 8A shows a TEM image of PMMA/silica nanocomposite particles (entry 12, Table 1) after removal of the organic polymer component and Figure 8B depicts an SEM image of P(MMA-BuA)/silica nanocomposite particles (entry 5, Table 2) after calcination. Both images confirm the presence of hollow contiguous silica shells. The SEM image in Figure 8B indicates that the silica shells of the nanocomposite particles are in direct contact with each other. Since a silica monolayer surrounds each nanocomposite

particle, a silica bilayer is inevitably formed upon drying. In contrast, the silica component of the same PMMA/silica nanocomposite particles (entry 12, Table 1) can be readily (and selectively) digested using excess concentrated NaOH. Once the silica has been etched away, latex-like particles are obtained that exhibit relatively smooth surfaces compared to those of the original nanocomposite particles. Moreover, there is no evidence for any silica particles inside these ‘latexes’. These observations suggest that the nanocomposite particles possess a well-defined ‘core-shell’ morphology with particulate silica shells and (co)polymer cores. This conclusion is also supported by small-angle x-ray scattering studies, which will be reported elsewhere in due course.

### **Optical Transmission of Nanocomposite Films**

The optical properties of 50:50 poly(styrene-co-n-butyl acrylate)/silica nanocomposite films of 76 to 330  $\mu\text{m}$  thickness have been previously assessed by visible absorption spectroscopy using a 50:50 copolymer latex film as a reference.<sup>10</sup> High transmission (> 80 %) was observed for nanocomposite films of less than 280  $\mu\text{m}$ , at least for visible wavelengths greater than 500 nm. In the present work, aqueous dispersions of various nanocomposite particles were dried in PVC molds at 30 °C, leading to free-standing nanocomposite films; mean film thicknesses were determined using a micrometer screw gauge. Flexible, highly transparent free-standing films were obtained for copolymer compositions of 50 wt. % BuA or greater (see Figure S4, Supporting Information). The mid-point glass transition temperature for a 50:50 P(MMA-BuA)/silica nanocomposite film was determined to be 21.7 °C by differential scanning calorimetry.

UV-visible absorption spectra were recorded for 50:50, 40:60 and 30:70 P(MMA-BuA)/silica nanocomposite films and also a 50:50 poly(styrene-co-n-butyl acrylate)/silica film, see Figure 9. The latter reference sample had a silica content of 39 wt. %, whereas the P(MMA-BuA)/silica films had silica contents of 26, 33 and 39 wt. %, respectively. It is emphasized that these four nanocomposite films had comparable thicknesses of approximately 250  $\mu\text{m}$ . Transmission for the three acrylic nanocomposite films exceeded 80 % over the 500 – 1100 nm range. This excellent optical transparency indicates that the 18 nm silica particles are homogeneously dispersed at the nano scale within each film. Moreover, the silica content of the films does not appear to strongly influence their transmission, at least over this spectral range. It is also noteworthy that the transparency of a 50:50 P(MMA-BuA) copolymer latex film prepared using APS initiator and an anionic surfactant (sodium n-dodecyl sulfate, 1.0

wt. % based on monomer) is actually significantly less transparent than the equivalent nanocomposite film (see Figure S5, Supporting Information). This is presumably due to the presence of excess surfactant within the film. The incorporation of BuA comonomer is essential for both film formation and film transparency; nanocomposite particles with relatively low BuA contents (< 50 wt. %) merely produced cracked, opaque films after solvent casting, whereas higher BuA contents led to good-quality resilient films with much greater optical clarity. Another important difference is that films cast from the all-acrylic formulation transmit light much better at UV wavelengths (e.g. 71 % transmittance at 300 nm) compared to the styrene-based copolymer/silica nanocomposite film, which only has a transmittance of 3 % at this wavelength. This reduced transmittance is simply due to the strong uv absorption by the aromatic chromophore in the styrene repeat units.

### **Particle Formation Mechanism**

Aliquots were withdrawn during ‘scaled-up’ syntheses of PMMA/silica nanocomposite particles and analyzed via several techniques to examine the mechanism of particle formation. Polymerizations initiated with both 1.0 and 3.0 wt. % AIBA initiator (based on monomer mass) were conducted; Figure 10 shows the evolution of DLS particle diameter and monomer conversion (determined by gravimetric analysis) with time. As previously observed for polystyrene/silica particles,<sup>29</sup> there is a good correlation between the DLS particle diameter and monomer conversion. During the synthesis performed with 3.0 % initiator, the monomer conversion reaches an initial plateau after 45 minutes (85 % conversion), then increased more slowly over time to attain a final conversion of 96 %. The evolution of DLS particle diameter closely follows the monomer conversion: a diameter of ~330 nm is reached after 45 min, followed by a gradual increase in size to the final diameter of approximately 370 nm. As expected, the polymerization proceeded at a slower rate when the lower initiator concentration was used, reaching a conversion of 95 % and particle diameter of 370 nm after 8 h at 60 °C.

Selected aliquots extracted from the reaction solution were analyzed by TEM: images obtained at various monomer conversions are shown in Figure 11. At the start of the polymerization (0 % conversion) only ultrafine silica particles are observed by TEM, with DLS studies confirming the intensity-average particle diameter to be that of the pristine silica sol (26 nm). At a monomer conversion of just 2 %, nascent particles can be observed; these are rather small (~50 nm) and are surrounded by the excess free silica. The mean particle size

increases monotonically with conversion (from 2 % through to 90 %) with excess silica being observed in all cases. Bearing in mind polydispersity effects, the DLS diameters are consistent with those observed by TEM suggesting that little or no flocculation occurs during the polymerization. The proportion of excess silica progressively decreases over time, due to its adsorption onto the surface of the growing nanocomposite particles. At the end of the polymerization (after 24 h) the nanocomposite particles are well-coated by silica, with very little free silica being observed by TEM provided that an optimized formulation is utilized.

DCP is a high resolution particle sizing technique that has been widely used in colloid science to size a range of lyophobic colloids including silica,<sup>53</sup> carbon nanotubes,<sup>54</sup> a range of copolymer latexes,<sup>55,56</sup> gold sols<sup>57,58</sup> and various nanocomposite particles.<sup>10,14,16,18,29,32,39,59,60</sup> In addition, DCP can be used to probe the colloidal stability of particulate dispersions. For example, incipient flocculation induced by either the physical adsorption of silica nanoparticles<sup>9</sup> or the deposition of an ultrathin overlayer of a conducting polymer is readily detected.<sup>61-63</sup> For example, Colard et al. monitored the depletion of an ultrafine silica sol from the reaction solution during the in situ formation of polymer/silica colloidal nanocomposite particles.<sup>53</sup> However, one drawback associated with DCP is that a single value for particle density must be determined and input into the software to obtain meaningful size distributions. This is usually overcome by measuring the bulk density of the dried particles using helium pycnometry. Clearly, this is not straightforward for the nanocomposite syntheses described herein, where the silica content (and hence particle density) may vary significantly for the growing monomer-swollen particles during the copolymerization.

DCP has been used to investigate the in situ formation of PMMA/silica nanocomposite particles. Aliquots withdrawn during polymerization were diluted and subsequently analyzed by this technique assuming a constant particle density of  $1.38 \text{ g cm}^{-3}$  (which is the final particle density). While this density inevitably leads to incorrect particle diameters at lower monomer conversions, the general trend in particle size and the extent of particle flocculation is nevertheless apparent. Figure 12 shows weight-average particle size distributions obtained for aliquots taken at increasing monomer conversion for two kinetic runs. Figure 12A depicts a nanocomposite synthesis conducted with sufficient silica to form colloidally stable particles. In contrast, Figure 12B represents the situation when the initial silica concentration is not quite sufficient to fully stabilize the nanocomposite particles, leading to a flocculated final dispersion. In both cases nascent particles can be detected at just 2 % monomer conversion.

These nuclei rapidly grow with increasing monomer conversion, which is consistent with the DLS and TEM studies discussed above. The key differences between these two syntheses first become apparent at monomer conversions above 20 %. The particle size distributions in Figure 12A remain narrow with increasing monomer conversion, with the mean particle diameter becoming fairly constant after approximately 74 % conversion. The secondary peak observed at higher diameter exhibits some fluctuation in intensity. Nevertheless, it is clear that the nanocomposite particles remain both relatively monodisperse and colloidally stable, regardless of the monomer conversion. This is manifestly not the case in Figure 12B; at 28 % monomer conversion and above the particles become progressively more flocculated. This is due to the relatively low silica concentration used in this formulation, with aggregation most likely occurring due to incomplete coverage of the growing nanocomposite particles with silica.

The effect of adding additional silica to the flocculated PMMA/silica particles after the polymerization was also studied. This was to investigate whether it is possible to optimize the post-reaction colloidal stability. Additional silica was added to the flocculated nanocomposite particles (5, 27 or 53 wt. % silica based on the mass of nanocomposite particles), followed by sonication and subsequent analysis by DCP (see Figure S6, Supporting Information). If all of the added silica was adsorbed, the final silica contents of the nanocomposite particles should be 20, 33 and 45 wt. % respectively. These values correspond to silica contents at which the final nanocomposite particle dispersions usually have (a) too little silica, (b) just enough silica with very little excess and (c) excess silica. Although the degree of flocculation could be reduced by the addition of excess silica (as judged by DCP), a substantial fraction of doublets and triplets remained. This suggests that, if the particles flocculate during polymerization, redispersion is relatively difficult to achieve.

The mechanism of nanocomposite formation involves at least three steps: particle nucleation, growth of monomer-swollen partially coated particles and silica adsorption; this sequence is summarized in Figure 13. In the early stages of the polymerization, small nascent particles are formed. The cationic AIBA initiator adsorbs onto the anionic silica particles at a saturation coverage of  $0.045 \text{ mg m}^{-2}$  (at  $20 \text{ }^\circ\text{C}$ ).<sup>29</sup> In the present study this suggests that all of the silica particles are fully covered with initiator and substantial amounts of non-adsorbed AIBA are also present in the aqueous phase. The adsorbed initiator will decompose to form radicals which cause both surface and solution polymerization of MMA. This presumably

generates hydrophobic patches on the surface of the silica nanoparticles which then aggregate to form the nascent nanocomposite particles. After nucleation, MMA diffuses from the metastable silica-stabilized monomer droplets (typically 280  $\mu\text{m}$ , as determined by laser diffraction) and polymerization then takes place inside the growing monomer-swollen nanocomposite particles. On swelling, the surface area of these particles increases and some silica nanoparticles subsequently adsorb onto the bare patches on the nanocomposite surface. Once high MMA conversion (~80 %) is attained, the particles reach their final particle size. However, there is still some free silica present in the solution. These remaining silica nanoparticles gradually adsorb onto and fully coat the surface of the nanocomposite particles leading to full monolayer coverage and high final colloidal stability.

## **Conclusions**

The efficient synthesis of all-acrylic colloidal nanocomposite particles via the in situ aqueous emulsion copolymerization of methyl methacrylate with n-butyl acrylate in the presence of a glycerol-functionalized silica sol using a cationic azo initiator is reported. Control experiments conducted using a non-functionalized silica sol or with anionic persulfate initiator do not lead to successful nanocomposite particle formation. Copolymer/silica nanocomposite particles with weight-average diameters ranging from 140 to 330 nm were obtained with silica contents varying from 20 to 39 % by mass. High monomer conversions and silica aggregation efficiencies can be achieved by optimizing the formulation. These nanocomposite particles have copolymer cores and particulate silica shells, as judged by transmission electron microscopy, aqueous electrophoresis and x-ray photoelectron spectroscopy. Films cast from n-butyl acrylate-rich copolymer/silica nanocomposite dispersions are significantly more transparent than films of comparable thickness prepared from the poly(styrene-co-n-butyl acrylate)/silica nanocomposite particles reported previously, particularly at shorter wavelengths (300-500 nm). The mechanism of particle formation involves (i) nucleation, (ii) growth of monomer-swollen particles partially coated with silica and (iii) silica adsorption in the final stages to attain monolayer coverage and form well-defined core-shell nanocomposite particles.

## **Acknowledgments**

The University of Sheffield is thanked for funding a PhD studentship for LAF. Dr. J. A. Owen is acknowledged for TEM assistance, Dr. C. Hurley performed the XPS studies and Dr. P. Greenwood is thanked for donation of the silica sols.

## References

- (1) Xue, Z.; Wiese, H. **2006**, United States Patent US7094830B2.
- (2) BASF-Corporation, [www.col9.com](http://www.col9.com) (accessed on 21/10/2010).
- (3) Bourgeat-Lami, E. J. *Nanosci. Nanotechnol.* **2002**, 2, 1.
- (4) Balmer, J. A.; Schmid, A.; Armes, S. P. *J. Mater. Chem.* **2008**, 18, 5722.
- (5) Zou, H.; Wu, S. S.; Shen, J. *Chem. Rev.* **2008**, 108, 3893.
- (6) Wang, T.; Keddie, J. L. *Adv. Colloid Interface Sci.* **2009**, 147-148, 319.
- (7) Balmer, J. A.; Armes, S. P.; Fowler, P. W.; Tarnai, T.; Gaspar, Z.; Murray, K. A.; Williams, N. S. *J. Langmuir* **2009**, 25, 5339.
- (8) Balmer, J. A.; Mykhaylyk, O. O.; Fairclough, J. P. A.; Ryan, A. J.; Armes, S. P.; Murray, M. W.; Murray, K. A.; Williams, N. S. *J. Am. Chem. Soc.* **2010**, 132, 2166.
- (9) Balmer, J. A.; Le Cunff, E. C.; Armes, S. P. *Langmuir* **2010**, 26, 13662.
- (10) Schmid, A.; Scherl, P.; Armes, S. P.; Leite, C. A. P.; Galembeck, F. *Macromolecules* **2009**, 42, 3721.
- (11) Chen, M.; Wu, L. M.; Zhou, S. X.; You, B. *Macromolecules* **2004**, 37, 9613.
- (12) Gill, M.; Mykytiuk, J.; Armes, S. P.; Edwards, J. L.; Yeates, T.; Moreland, P. J.; Mollett, C. J. *Chem. Soc. Chem. Commun.* **1992**, 108.
- (13) Maeda, S.; Armes, S. P. *J. Colloid Interface Sci.* **1993**, 159, 257.
- (14) Han, M. G.; Armes, S. P. *Langmuir* **2003**, 19, 4523.
- (15) Barthet, C.; Hickey, A. J.; Cairns, D. B.; Armes, S. P. *Adv. Mater.* **1999**, 11, 408.
- (16) Percy, M. J.; Barthet, C.; Lobb, J. C.; Khan, M. A.; Lascelles, S. F.; Vamvakaki, M.; Armes, S. P. *Langmuir* **2000**, 16, 6913.
- (17) Amalvy, J. I.; Percy, M. J.; Armes, S. P.; Wiese, H. *Langmuir* **2001**, 17, 4770.
- (18) Percy, M. J.; Michailidou, V.; Armes, S. P.; Perruchot, C.; Watts, J. F.; Greaves, S. J. *Langmuir* **2003**, 19, 2072.
- (19) Maeda, S.; Gill, M.; Armes, S. P.; Fletcher, I. W. *Langmuir* **1995**, 11, 1899.
- (20) Butterworth, M. D.; Corradi, R.; Johal, J.; Lascelles, S. F.; Maeda, S.; Armes, S. P. *J. Colloid Interface Sci.* **1995**, 174, 510.
- (21) Percy, M. J.; Amalvy, J. I.; Barthet, C.; Armes, S. P.; Greaves, S. J.; Watts, J. F.; Wiese, H. *J. Mater. Chem.* **2002**, 12, 697.
- (22) Agarwal, G. K.; Titman, J. J.; Percy, M. J.; Armes, S. P. *J. Phys. Chem. B* **2003**, 107, 12497.
- (23) Amalvy, J. I.; Percy, M. J.; Armes, S. P.; Leite, C. A. P.; Galembeck, F. *Langmuir* **2005**, 21, 1175.
- (24) Luna-Xavier, J.-L.; Bourgeat-Lami, E.; Guyot, A. *Colloid Polymer Science* **2001**, 279, 947.
- (25) Luna-Xavier, J.-L.; Guyot, A.; Bourgeat-Lami, E. *J. Colloid Interface Sci.* **2002**, 250, 82.
- (26) Reculosa, S.; Mingotaud, C.; Bourgeat-Lami, E.; Duguet, E.; Ravaine, S. *Nano Lett.* **2004**, 4, 1677.
- (27) Chen, M.; Zhou, S.; You, B.; Wu, L. *Macromolecules* **2005**, 38, 6411.
- (28) Cheng, C. M.; Micala, F. J.; Vanderhoff, J. W.; Elaasser, M. S. *J. Polym. Sci., Part A: Polym. Chem.* **1992**, 30, 235.
- (29) Schmid, A.; Armes, S. P.; Leite, C. A. P.; Galembeck, F. *Langmuir* **2009**, 25, 2486.
- (30) Dupin, D.; Schmid, A.; Balmer, J. A.; Armes, S. P. *Langmuir* **2007**, 23, 11812.
- (31) Colver, P. J.; Colard, C. A. L.; Bon, S. A. F. *J. Am. Chem. Soc.* **2008**, 130, 16850.
- (32) Percy, M. J.; Armes, S. P. *Langmuir* **2002**, 18, 4562.

- (33) Percy, M. J.; Amalvy, J. I.; Randall, D. P.; Armes, S. P.; Greaves, S. J.; Watts, J. F. *Langmuir* **2004**, *20*, 2184.
- (34) Bourgeat-Lami, E.; Lang, J. J. *Colloid Interface Sci.* **1998**, *197*, 293.
- (35) Bourgeat-Lami, E.; Lang, J. J. *Colloid Interface Sci.* **1999**, *210*, 281.
- (36) Bourgeat-Lami, E.; Lang, J. *Macromol. Symp.* **2000**, *151*, 377.
- (37) Yoshinaga, K.; Yokoyama, T.; Sugawa, Y.; Karakawa, H.; Enomoto, N.; Nishida, H.; Komatsu, M. *Polym. Bull.* **1992**, *28*, 663.
- (38) Schmid, A.; Fujii, S.; Armes, S. P. *Langmuir* **2006**, *22*, 4923.
- (39) Schmid, A.; Fujii, S.; Armes, S. P. *Langmuir* **2005**, *21*, 8103.
- (40) Schmid, A.; Fujii, S.; Armes, S. P.; Leite, C. A. P.; Galembeck, F.; Minami, H.; Saito, N.; Okubo, M. *Chem. Mater.* **2007**, *19*, 2435.
- (41) Cheng, X. J.; Chen, M.; Zhou, S. X.; Wu, L. M. *J. Polym. Sci., Part A: Polym. Chem.* **2006**, *44*, 3807.
- (42) Qi, D. M.; Bao, Y. Z.; Huang, Z. M.; Weng, Z. X. *Colloid Polymer Science* **2008**, *286*, 233.
- (43) Keddie, J. L. *Materials Science & Engineering R-Reports* **1997**, *21*, 101.
- (44) Iler, R. K. *The Chemistry of Silica*; John Wiley & Sons, Inc.: New York, 1979.
- (45) Fujii, S.; Armes, S. P.; Binks, B. P.; Murakami, R. *Langmuir* **2006**, *22*, 6818.
- (46) Schmid, A.; Tonnar, J.; Armes, S. P. *Adv. Mater.* **2008**, *20*, 3331.
- (47) Tiarks, F.; Landfester, K.; Antonietti, M. *Langmuir* **2001**, *17*, 5775.
- (48) Zhou, J.; Zhang, S. W.; Qiao, X. G.; Li, X. Q.; Wu, L. M. *J. Polym. Sci., Part A: Polym. Chem.* **2006**, *44*, 3202.
- (49) Qi, D. M.; Bao, Y. Z.; Weng, Z. X.; Huang, Z. M. *Polymer* **2006**, *47*, 4622.
- (50) Greenwood, P.; Lagnemo, H. **2004**, WO2004/035474A1.
- (51) Lee, D.; Balmer, J. A.; Schmid, A.; Tonnar, J.; Armes, S. P.; Titman, J. J. *Langmuir* **2010**, *26*, 15592.
- (52) Beamson, G.; Briggs, D. *High Resolution XPS of Organic Polymers*; John Wiley & Sons: Chichester, 1992.
- (53) Colard, C. A. L.; Teixeira, R. F. A.; Bon, S. A. F. *Langmuir* **2010**, *26*, 7915.
- (54) Nadler, M.; Mahrholz, T.; Riedel, U.; Schilde, C.; Kwade, A. *Carbon* **2008**, *46*, 1384.
- (55) Dupin, D.; Fujii, S.; Armes, S. P.; Reeve, P.; Baxter, S. M. *Langmuir* **2006**, *22*, 3381.
- (56) Thompson, K. L.; Armes, S. P.; York, D. W.; Burdis, J. A. *Macromolecules* **2010**, *43*, 2169.
- (57) Kohler, J. M.; Wagner, J.; Albert, J. J. *Mater. Chem.* **2005**, *15*, 1924.
- (58) Krpetic, Z.; Porta, F.; Caneva, E.; Dal Santo, V.; Scari, G. *Langmuir* **2010**, *26*, 14799.
- (59) Gill, M.; Armes, S. P.; Fairhurst, D.; Emmett, S. N.; Idzorek, G.; Pigott, T. *Langmuir* **1992**, *8*, 2178.
- (60) Maeda, S.; Armes, S. P. *J. Mater. Chem.* **1994**, *4*, 935.
- (61) Barthet, C.; Armes, S. P.; Lascelles, S. F.; Luk, S. Y.; Stanley, H. M. E. *Langmuir* **1998**, *14*, 2032.
- (62) Cairns, D. B.; Armes, S. P.; Bremer, L. G. B. *Langmuir* **1999**, *15*, 8052.
- (63) Schmid, A.; Sutton, L. R.; Armes, S. P.; Bain, P. S.; Manfre, G. *Soft Matter* **2009**, *5*, 407.

## List of Tables

### Table 1

Effect of varying the synthesis parameters on the mean density, silica content, silica aggregation efficiency and particle diameter of poly(methyl methacrylate)/silica nanocomposite particles prepared by aqueous emulsion polymerization at 60 °C using a commercial 18 nm silica sol (Bindzil CC40) and cationic AIBA initiator.<sup>a, b</sup>

### Table 2

Effect of varying the synthesis parameters on the mean density, silica content, silica aggregation efficiency and particle diameter of poly(methyl methacrylate-co-n-butyl acrylate)/silica nanocomposite particles prepared by aqueous emulsion copolymerization at 60 °C using a commercial 18 nm silica sol (Bindzil CC40) and cationic AIBA initiator.<sup>a</sup>

**Table 1.**

Entry number	Initial silica mass (g)	AIBA (mg)	Colloidal stability?	Particle density (g cm <sup>-3</sup> ) <sup>c</sup>	Silica content (wt. %) <sup>d</sup>	Silica aggregation efficiency (%) <sup>d</sup>	Weight-average diameter by DCP (nm)	Intensity-average diameter by DLS (nm)
1	0.0	50	N	-	-	-	-	-
2	0.5	50	N	-	-	-	-	-
3	1.0	50	N	-	-	-	-	-
4	1.5	50	Y	1.44	27	>99	194 ± 18	271 (0.012)
5	2.0	50	Y	1.44	28	99	194 ± 20	270 (0.032)
6	2.5	50	Y	1.42	29	81	195 ± 16	262 (0.024)
7	3.0	50	Y	1.36	30	70	195 ± 20	242 (0.005)
8	3.5	50	Y	1.37	25	49	202 ± 19	259 (0.016)
9	4.0	50	Y	1.37	26	43	195 ± 16	250 (0.018)
10	0.9	150	N	-	-	-	-	-
11	1.9	150	Y	1.41	29	>99	311 ± 38	582 (0.191)
12	2.3	150	Y	1.40	29	86	329 ± 49	468 (0.179)
13	2.8	150	Y	1.42	28	71	313 ± 42	350 (0.023)
14	3.2	150	Y	1.41	29	62	280 ± 36	321 (0.046)
15	3.7	150	Y	1.43	29	54	290 ± 37	397 (0.174)
16	4.2	150	Y	1.41	29	48	274 ± 35	351 (0.097)
17	2.5	25	Y	1.44	23	61	194 ± 17	257 (0.012)
18	2.5	100	Y	1.43	31	90	199 ± 21	247 (0.013)
19	2.5	150	Y	1.44	32	93	200 ± 22	246 (0.012)
20 <sup>e</sup>	2.5	50	N	-	-	-	-	-
21 <sup>f</sup>	2.5	50	N	-	-	-	-	-
22 <sup>g</sup>	2.5	50	N	-	-	-	-	-

<sup>a</sup> All polymerizations were conducted using 5.0 g total comonomer in a total reaction mass of 50 g at 60 °C for 24 h. <sup>b</sup> In most cases the final monomer conversion was greater than 90 %. <sup>c</sup> Determined by helium pycnometry. <sup>d</sup> Determined by thermogravimetric analysis. <sup>e</sup> Control experiment using non-functionalized Bindzil 2040 silica sol. <sup>f</sup> Control experiment using non-functionalized Ludox TM-40 silica sol. <sup>g</sup> Control experiment using anionic KPS initiator.

**Table 2.**

Entry number	Initial silica mass (g)	MMA:BuA mass ratio <sup>b</sup>	AIBA (mg)	Colloidal stability?	Particle density (g cm <sup>-3</sup> ) <sup>c</sup>	Silica content (wt. %) <sup>d</sup>	Silica aggregation efficiency (%) <sup>d</sup>	Weight-average diameter by DCP (nm)	Intensity-average diameter by DLS (nm)
1	2.8	90 : 10	150	Y	1.39	30	76	217 ± 15	268 (0.020)
2	2.8	80 : 20	150	Y	1.37	29	73	233 ± 19	272 (0.020)
3	2.8	70 : 30	150	Y	1.32	23	54	224 ± 23	276 (0.018)
4	2.8	60 : 40	150	Y	1.26	21	48	241 ± 24	272 (0.040)
5	2.8	50 : 50	150	Y	1.38	26	63	169 ± 18	243 (0.033)
6	2.8	40 : 60	150	Y	1.27	33	89	236 ± 24	254 (0.020)
7	2.8	30 : 70	150	N	-	-	-	-	-
8	3.7	30 : 70	150	Y	1.38	39	85	138 ± 15	180 (0.013)
9	0.9	50 : 50	150	N	-	-	-	-	-
10	1.4	50 : 50	150	N	-	-	-	-	-
11	1.9	50 : 50	150	Y	1.35	20	69	205 ± 22	294 (0.022)
12	2.3	50 : 50	150	Y	1.32	21	57	197 ± 16	260 (0.013)

<sup>a</sup> All copolymerizations were conducted using 5.0 g total (co)monomer in a total reaction mass of 50 g at 60 °C for 24 h. <sup>b</sup> In most cases monomer conversion was greater than 90 %. <sup>c</sup> Determined by helium pycnometry. <sup>d</sup> Determined by thermogravimetric analysis.

## List of Figures

### Figure 1

Schematic representation of the surfactant-free synthesis of colloidal nanocomposite particles by aqueous emulsion copolymerization of methyl methacrylate with n-butyl acrylate at 60 °C using a cationic azo initiator (AIBA) in the presence of a commercial ultrafine glycerol-functionalized aqueous silica sol (Bindzil CC40) as the sole stabilizing agent.

### Figure 2

Representative TEM images of poly(methyl methacrylate)/silica nanocomposite particles prepared by aqueous emulsion polymerization using a glycerol-functionalized 18 nm silica sol and a cationic azo initiator. Images A, B, C and D correspond to entries 19, 18, 5 and 6 in Table 1 respectively. Images A and B show the nanocomposite particles after excess silica sol has been carefully removed by repeated centrifugation-redispersion cycles. In contrast, images C and D were recorded for the non-purified diluted reaction solution. Higher initial silica sol concentrations lead to higher levels of excess non-aggregated silica sol being present after the polymerization.

### Figure 3

TEM images recorded for: (A) emulsion polymerization of methyl methacrylate initiated with AIBA in the absence of any silica sol (entry 1, Table 1); (B, C) emulsion polymerization of methyl methacrylate initiated with AIBA using non-functionalized 20 nm silica sols (Ludox TM-40 and Bindzil 2040) instead of the 18 nm glycerol-functionalized (Bindzil CC40) sol (entries 20 and 21, Table 1); (D) emulsion polymerization of methyl methacrylate initiated with an anionic KPS initiator instead of the cationic AIBA initiator (entry 22, table 1). These four control experiments were each prepared under conditions that were otherwise identical to those used for the successful nanocomposite formulations.

### Figure 4

Weight-average particle size distributions obtained for poly(methyl methacrylate-co-n-butyl acrylate)/silica nanocomposite particles (entries 1 – 6, Table 2) using disk centrifuge photosedimentometry. The centrifugation rate was 18,000 rpm and the spin fluid was constructed from a density gradient containing 8.0 to 24.0 wt. % aqueous sucrose solution. In each case nanocomposite particle densities were determined by helium pycnometry (see Table 2).

### Figure 5

Representative TEM images obtained for various poly(methyl methacrylate-co-n-butyl acrylate)/silica nanocomposite particles prepared by aqueous emulsion copolymerization using various comonomer mass ratios in the presence of a glycerol-functionalized 18 nm silica sol (entries 1 – 6, Table 2). Copolymerizations were conducted using 2.80 g silica sol, 5.0 g total (co)monomer and 150 mg AIBA initiator at 60 °C for 24 h. Increasing coalescence can be observed with increasing n-butyl acrylate content. Both DLS and DCP studies confirmed that no particle aggregation occurred prior to drying.

### Figure 6

Aqueous electrophoresis curves obtained for poly(methyl methacrylate)/silica (entry 6, Table 1) and 50:50 poly(methyl methacrylate-co-n-butyl acrylate)/silica (entry 5, Table 2) nanocomposite particles, as well as the pristine glycerol-functionalized silica sol (Bindzil CC40).

**Figure 7**

XPS survey spectra recorded for freeze-dried 50:50 poly(methyl methacrylate-co-n-butyl acrylate)/silica nanocomposite particles pressed onto indium foil (entry 5 in Table 2). The inset shows the peak-fitted C1s core-line spectrum, indicating the presence of C-C, C-O and C=O species.

**Figure 8**

(A) TEM image of poly(methyl methacrylate)/silica nanocomposite particles (entry 12, Table 1) after removal of the organic polymer component by calcination at 500 °C in air. (B) SEM image of poly(methyl methacrylate-co-n-butyl acrylate)/silica nanocomposite particles (entry 5, Table 2) obtained after calcination at 500 °C in air. Both images confirm the presence of hollow contiguous silica shells. (C and D) TEM images recorded for poly(methyl methacrylate)/silica nanocomposite particles (entry 12, Table 1) after selective removal of silica using concentrated NaOH. This chemical etch produces latex-like particles with smooth surfaces, in striking contrast to the relatively rough surface of the original nanocomposite particles.

**Figure 9**

UV-visible absorption spectra recorded in transmission mode for poly(methyl methacrylate-co-n-butyl methacrylate)/silica films (entries 5, 6 and 8 in Table 2) and a poly(styrene-co-n-butyl acrylate)/silica nanocomposite film with mean thicknesses of approximately 250 μm. The inset shows a digital photograph obtained for the 40:60 poly(methyl methacrylate-co-n-butyl methacrylate)/silica nanocomposite film to illustrate its excellent optical transparency.

**Figure 10**

Monomer conversion and particle growth curves obtained for the synthesis of poly(methyl methacrylate)/silica nanocomposite particles using (a) 3.0 % AIBA (▲) and (b) 1.0 % AIBA (■). The reaction conditions are based on a scaled-up formulation for entry 15 shown in Table 1.

**Figure 11**

TEM images of aliquots withdrawn during the scale-up synthesis of poly(methyl methacrylate)/silica nanocomposite particles. The aliquots were quenched in air prior to dilution in order to prepare TEM grids. The monomer conversion as judged by gravimetry is indicated on each image. The reaction conditions are based on a scaled-up formulation for entry 15 shown in Table 1.

**Figure 12**

Weight-average particle size distributions for poly(methyl methacrylate)/silica particles with increasing monomer conversion: (A) when the silica concentration is sufficient to obtain colloidally stable particles; (B) when too little silica is present, leading to flocculated particles. The formulations for (A) and (B) are based on scaled up versions of entries 15 and 11 in Table 1 respectively.

**Figure 13**

Schematic representation of the mechanism of formation of colloidally stable poly(methyl methacrylate)/silica particles. Blue circles indicate silica particles, orange regions show polymer and AIBA initiator is represented red '+'.

**Figure 1.**

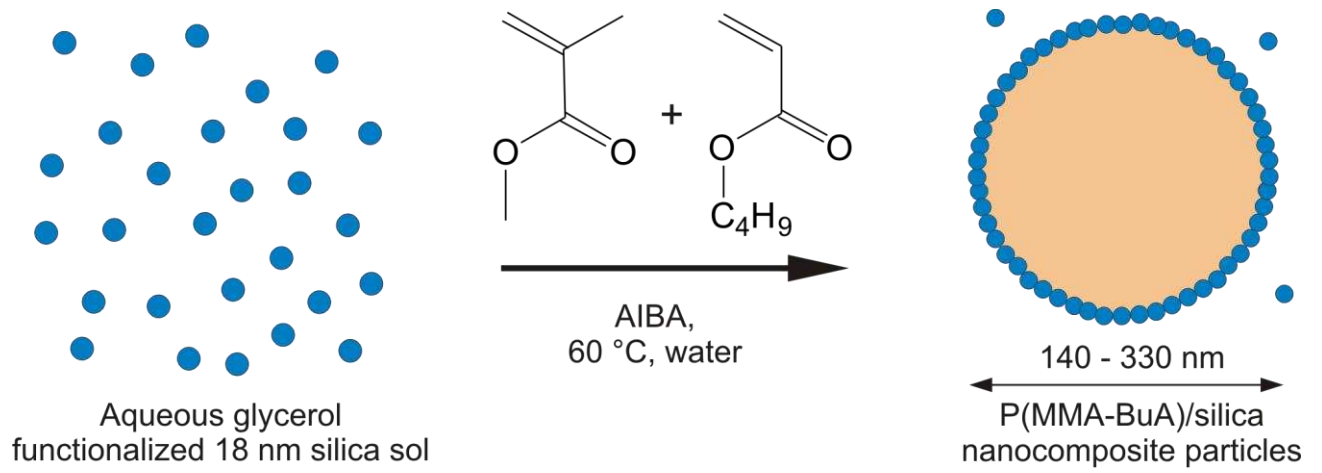


Figure 2.

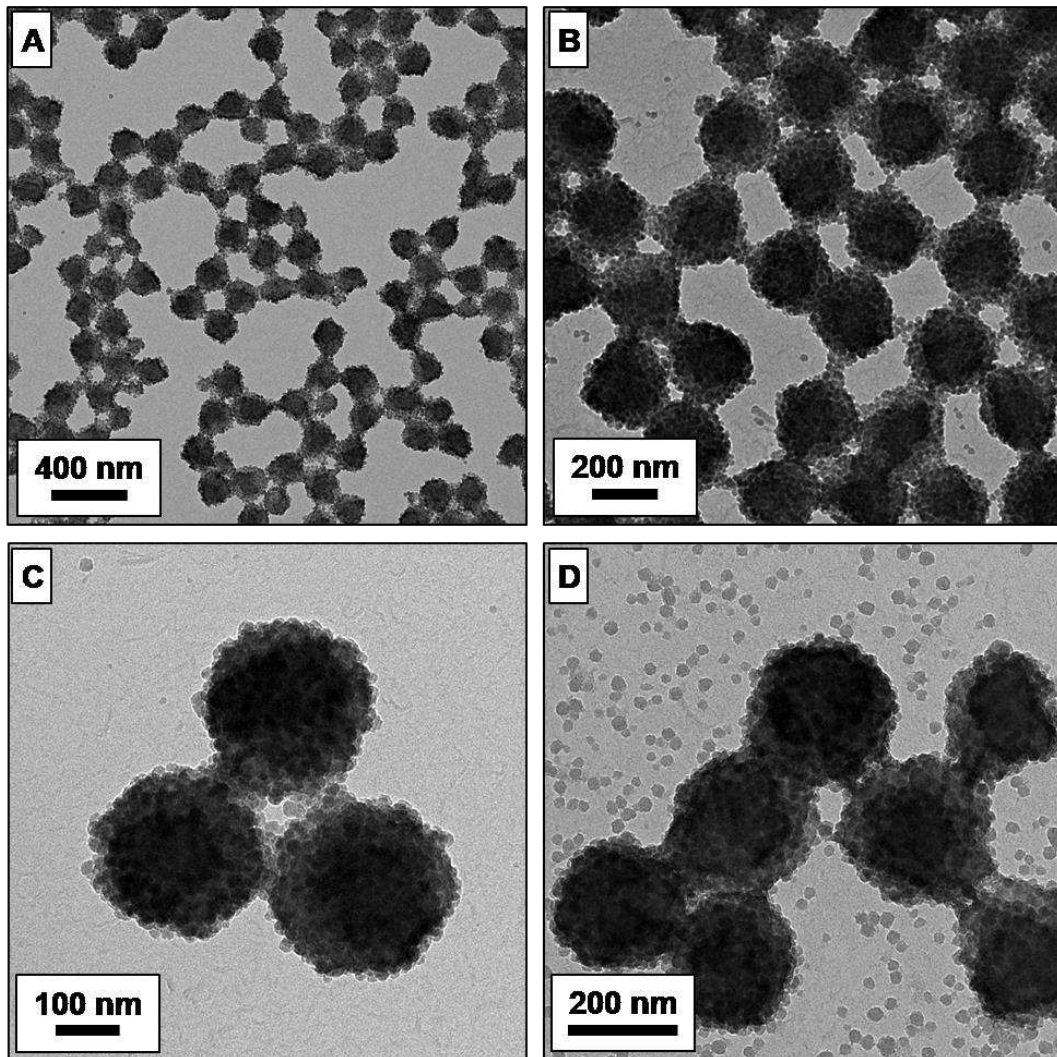


Figure 3.

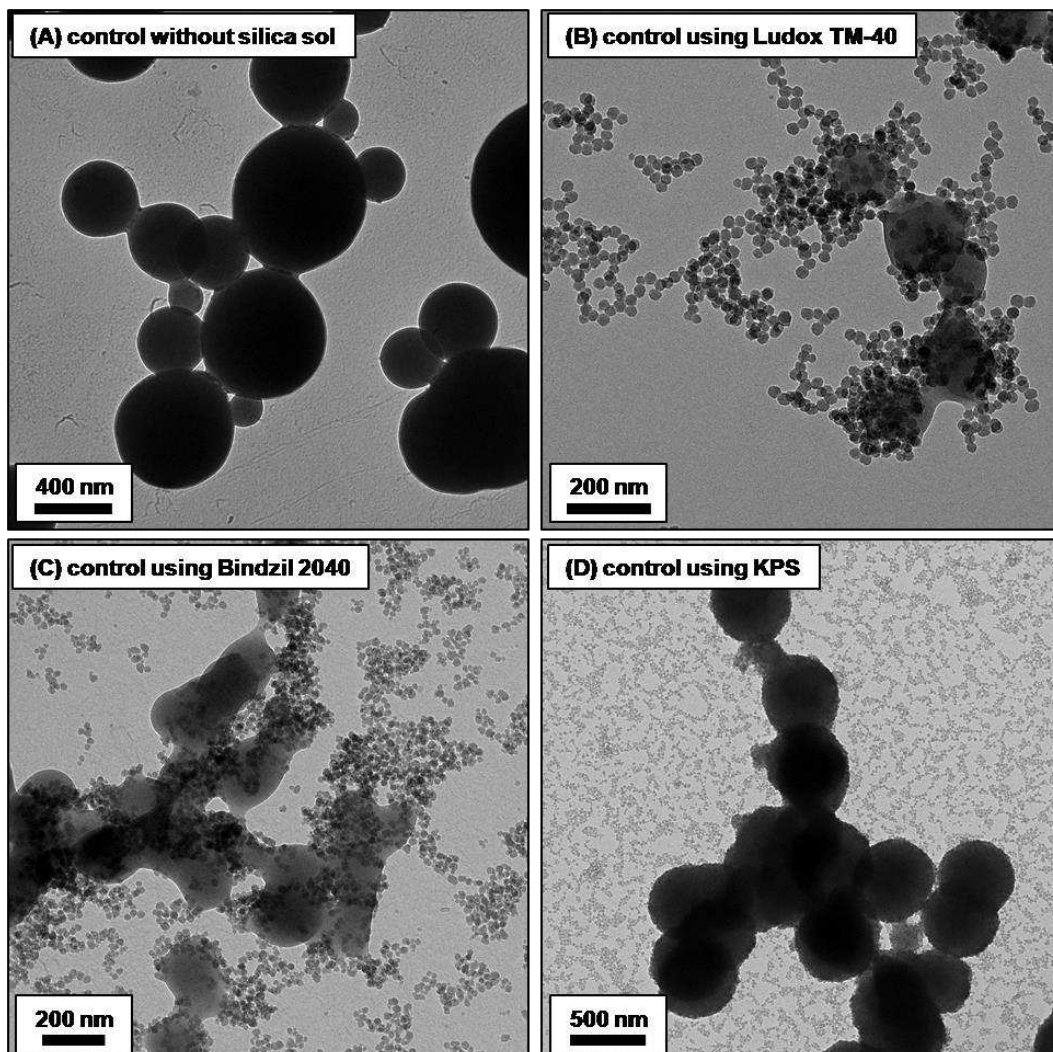


Figure 4.

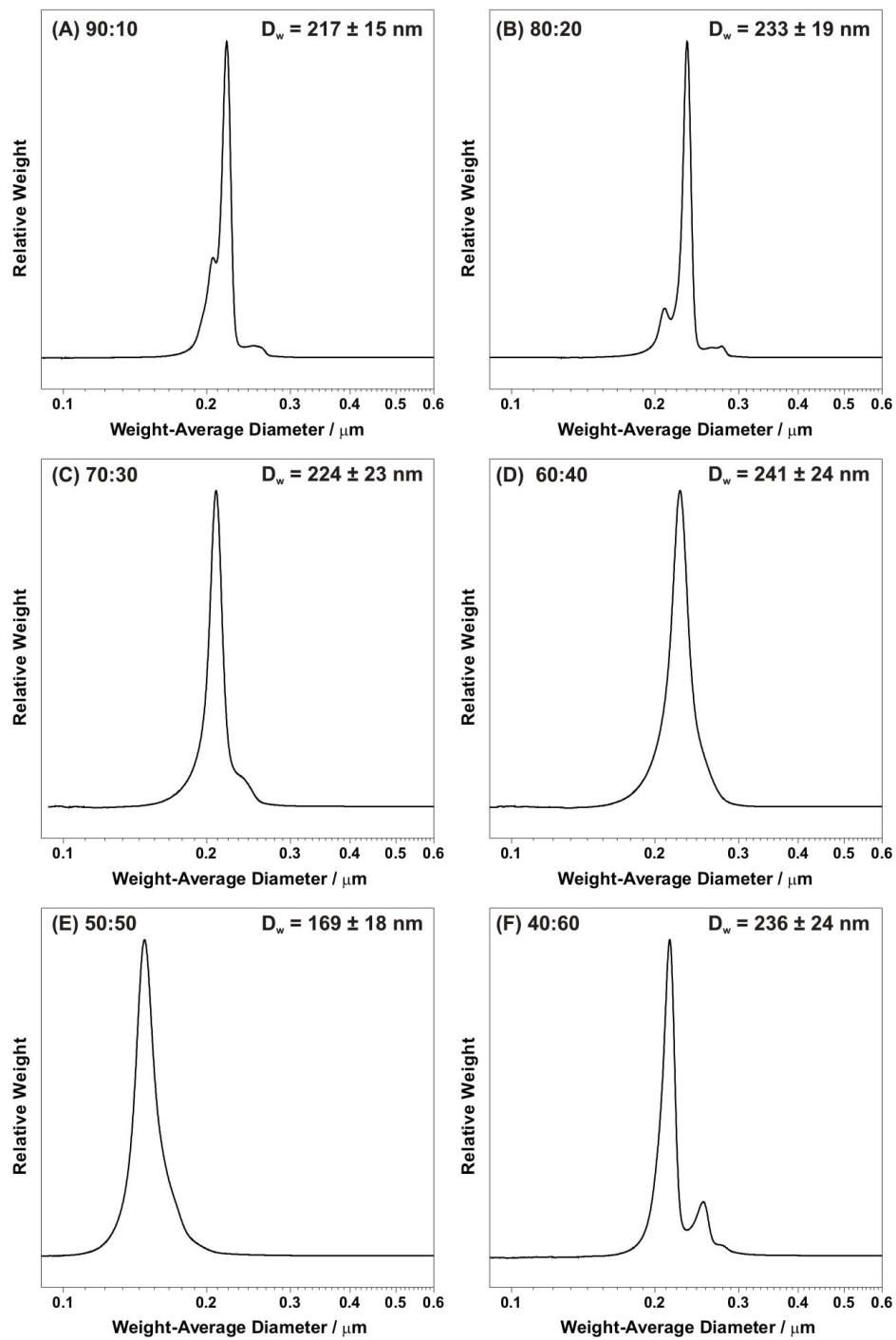


Figure 5.

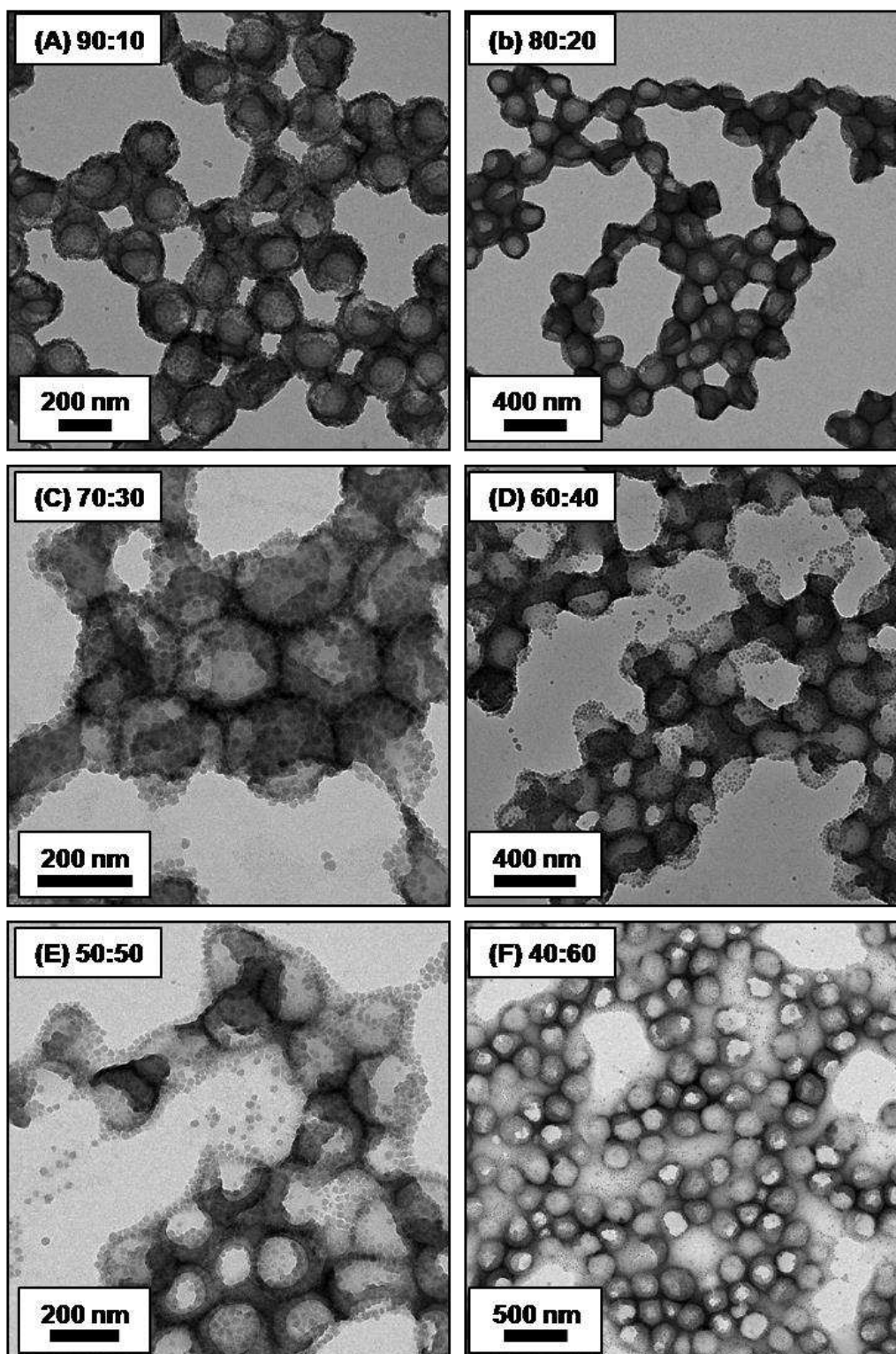
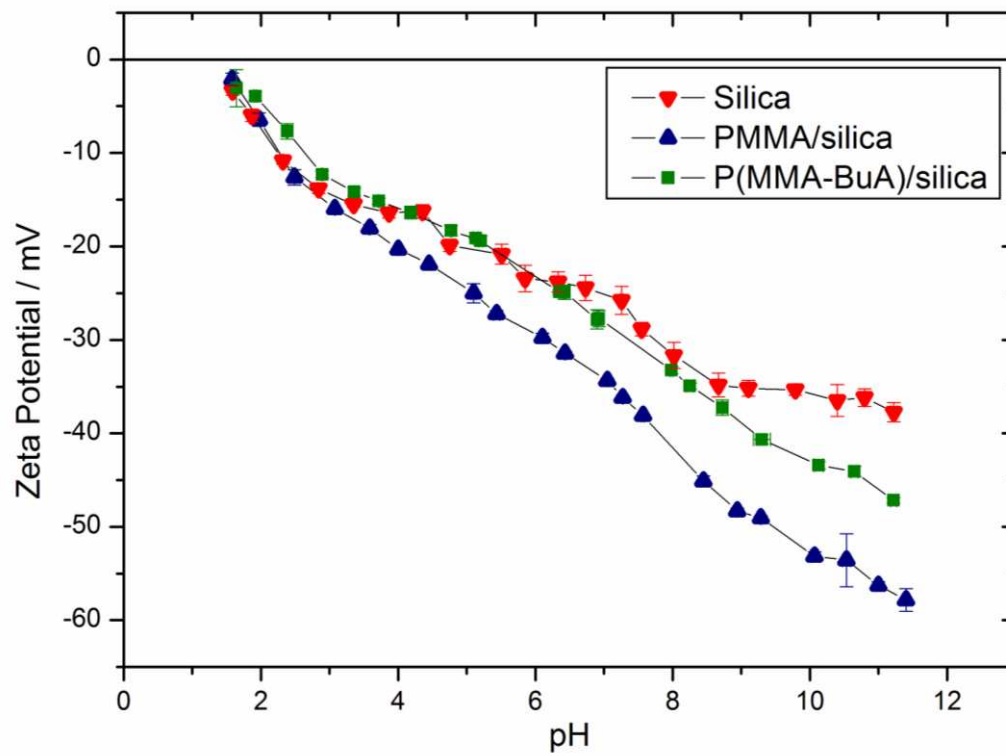


Figure 6.



**Figure 7.**

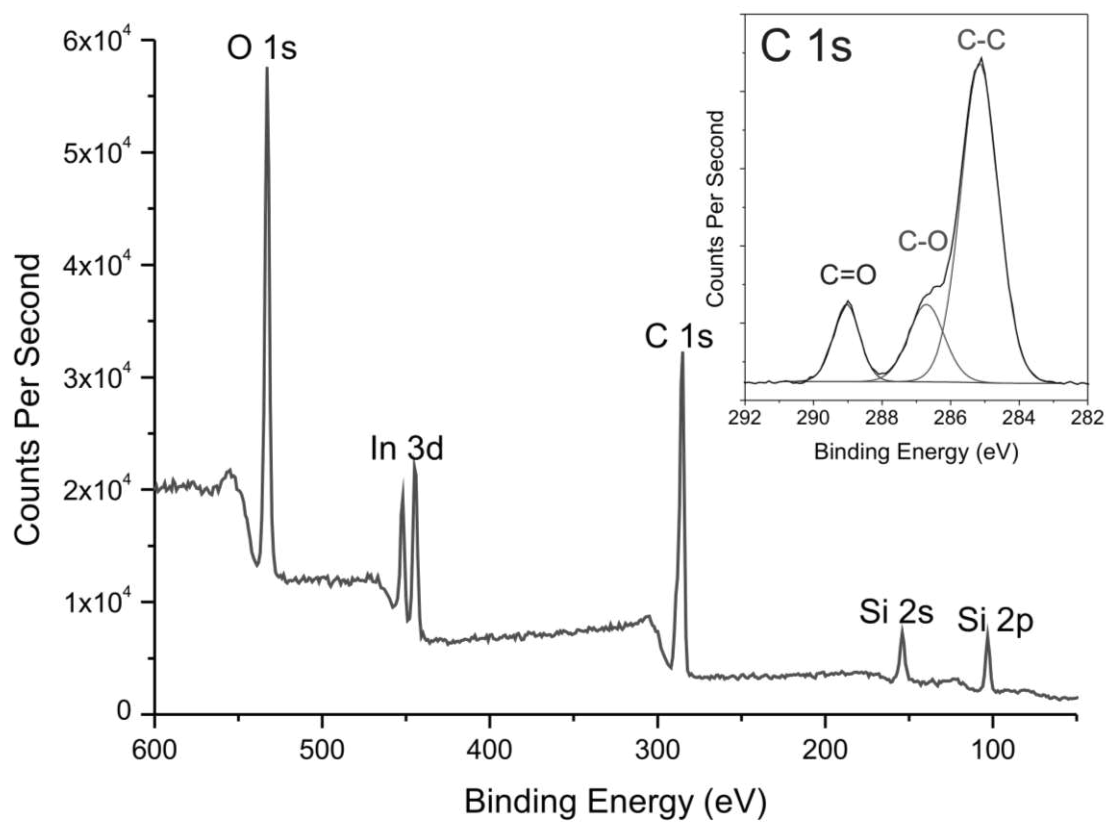
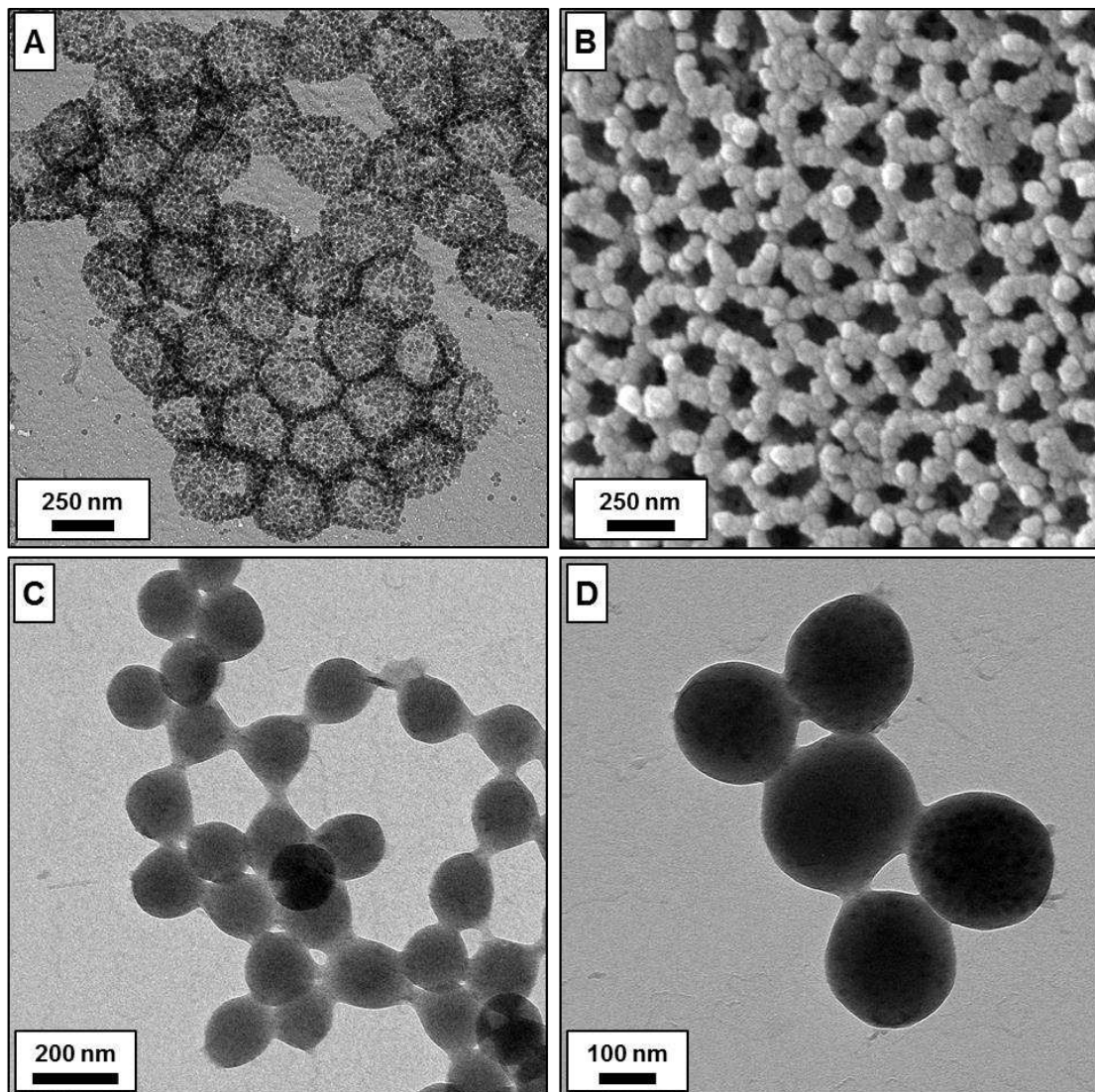


Figure 8.



**Figure 9.**

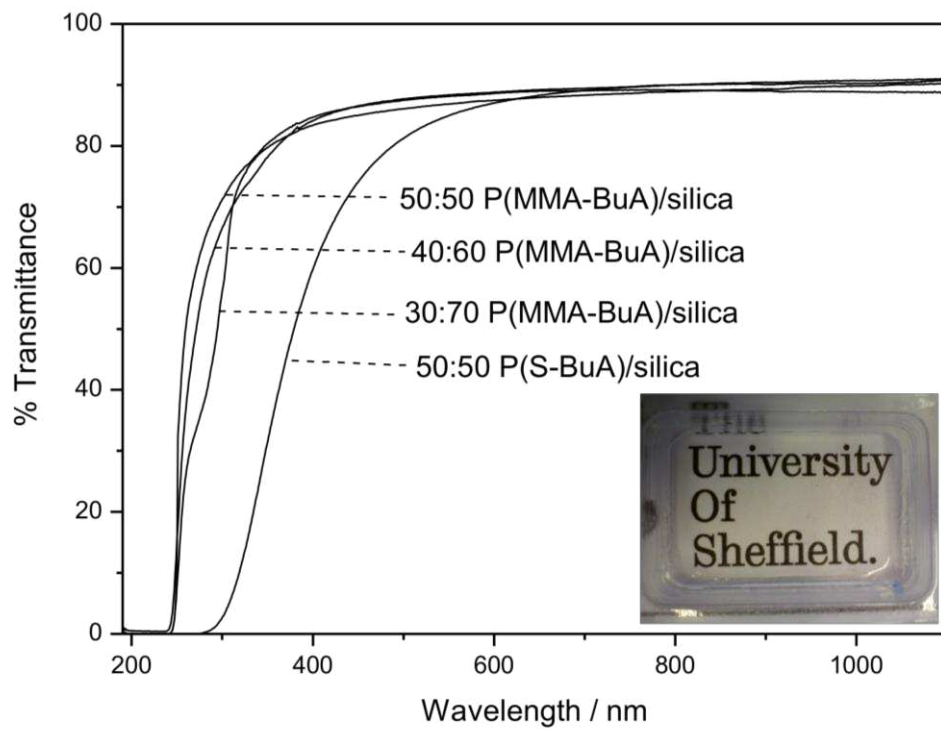


Figure 10.

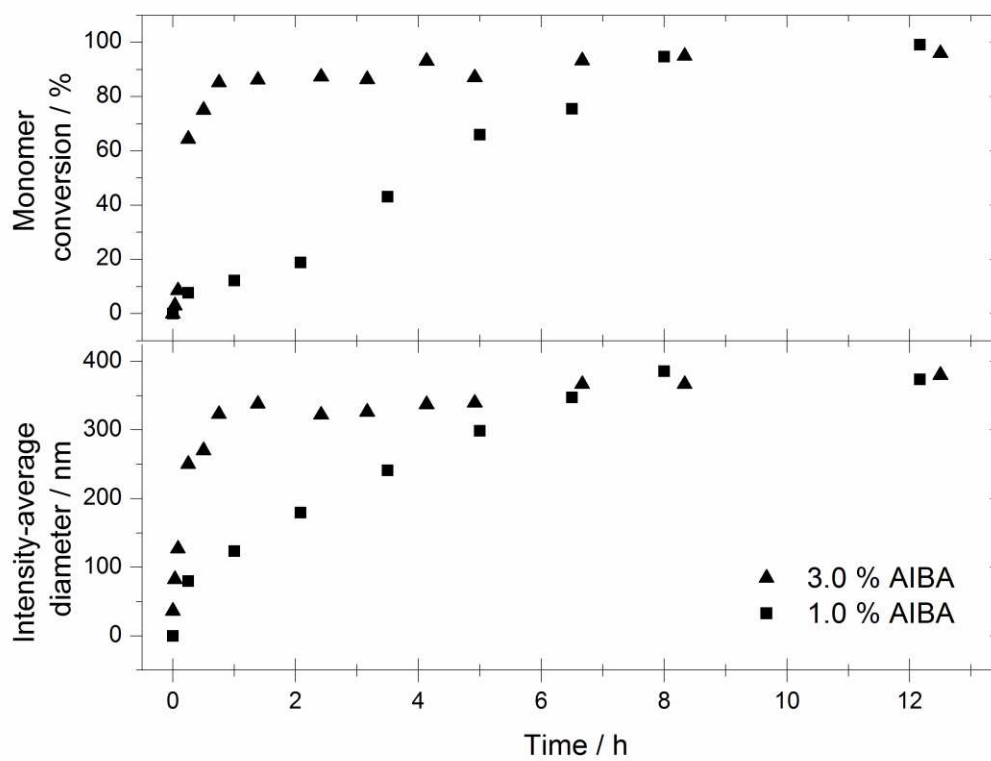


Figure 11.

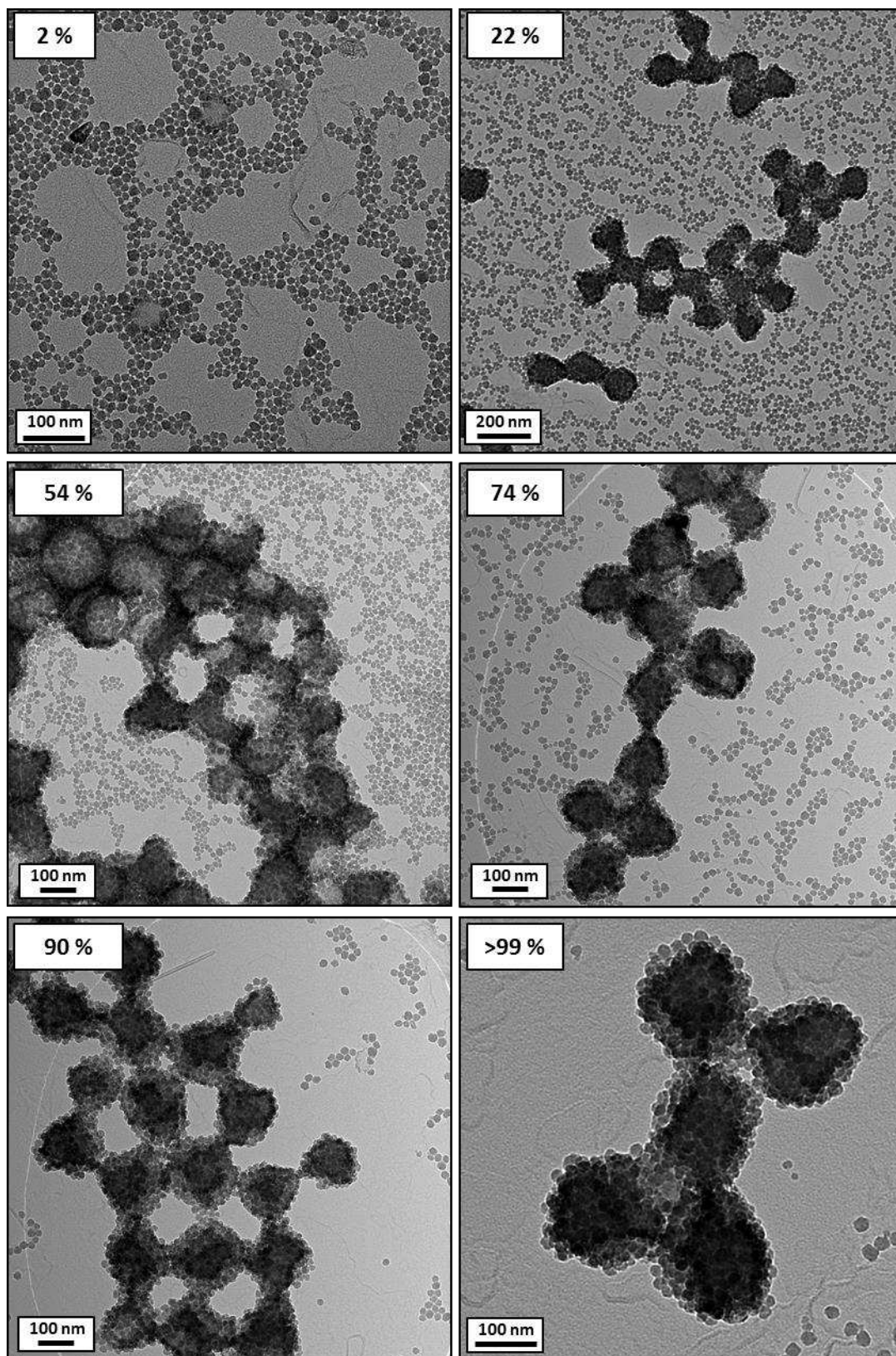


Figure 12.

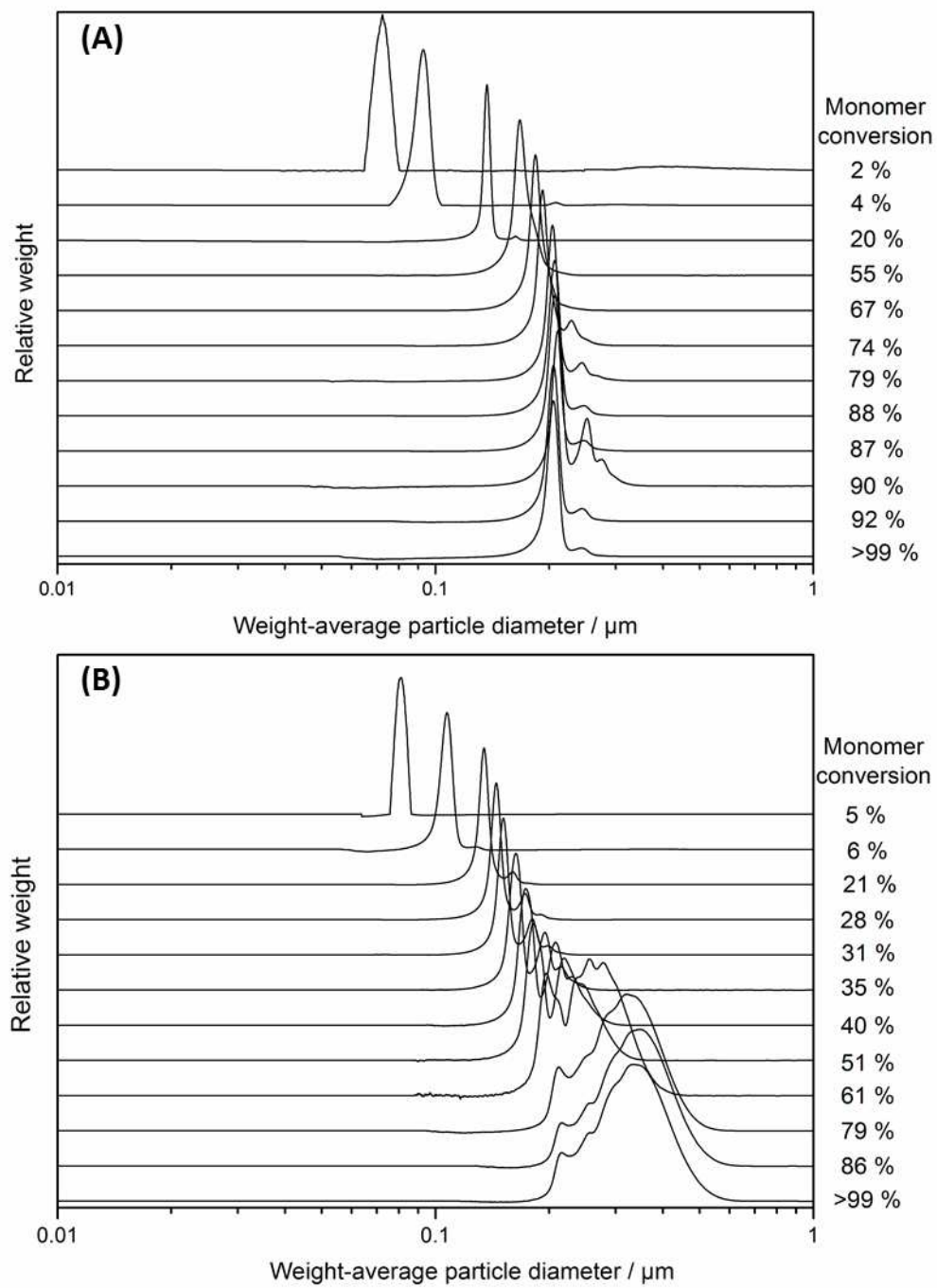
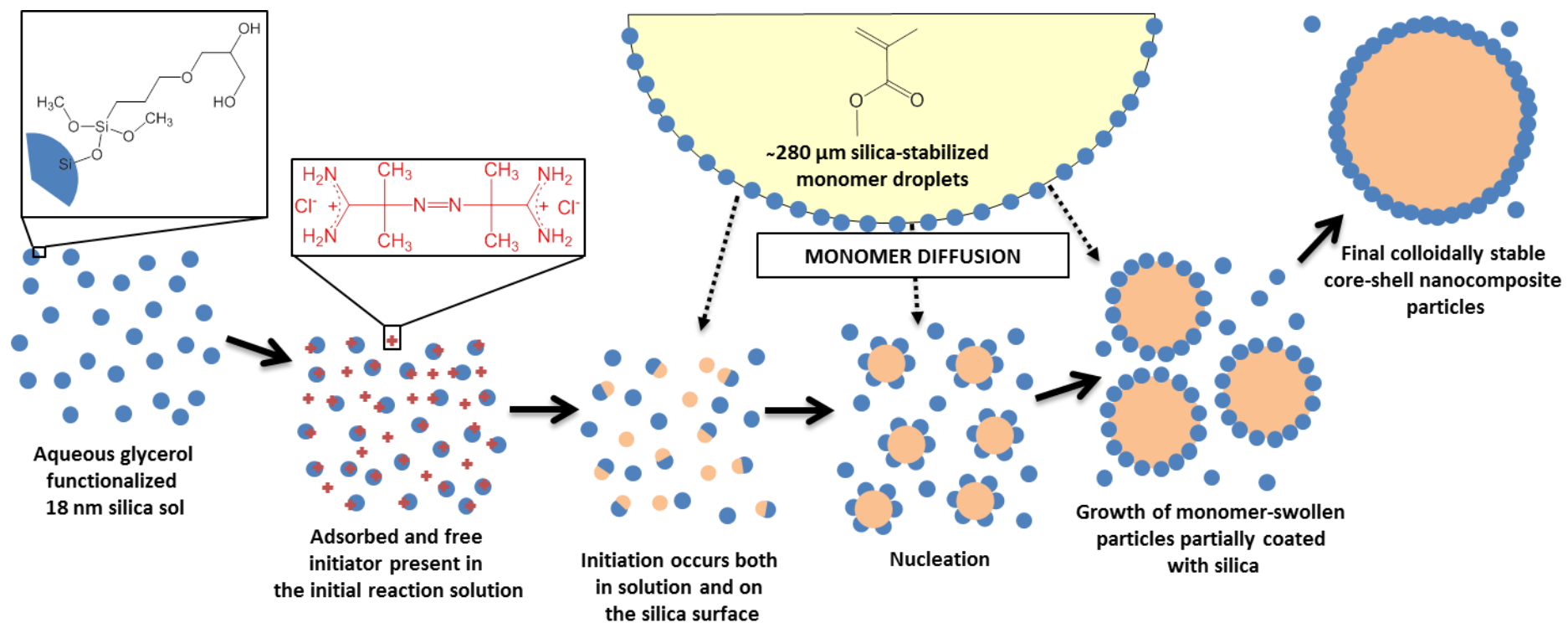
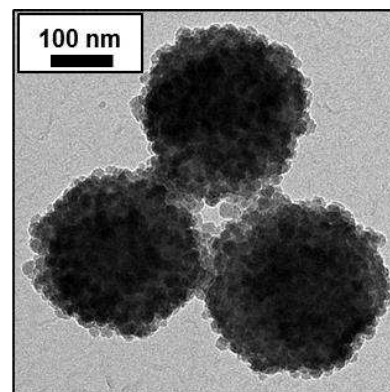
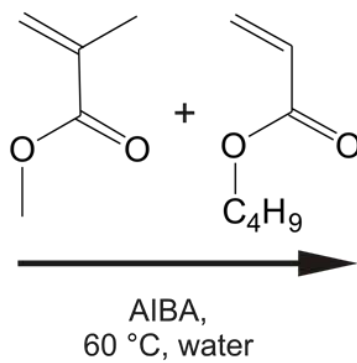
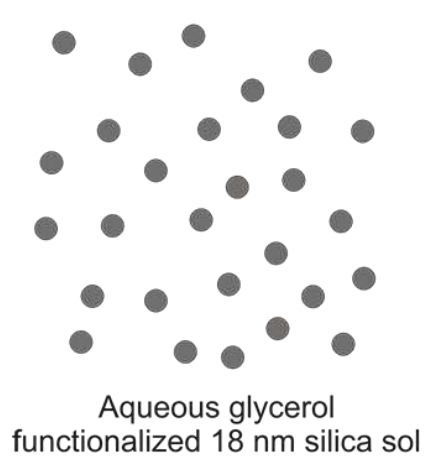


Figure 13.



## TOC Graphic



P(MMA-BuA)/silica  
nanocomposite particles